



OPEN

Electrochemical and DFT studies of *Terminalia bellerica* fruit extract as an eco-friendly inhibitor for the corrosion of steel

Ahmed M. Abuelela^{1,2✉}, Jasdeep Kaur³, Akhil Saxena^{3✉}, Mahmoud A. Bedair^{4✉}, Dakeshwar Kumar Verma⁵ & Elyor Berdimurodov^{6,7}

It is well known that metal corrosion causes serious economy losses worldwide. One of the most effective ways to prevent corrosion is the continuous development of high-efficient and environment-friendly corrosion inhibitors. Among the widely used organic and inorganic corrosion inhibitors, plant extracts are top candidates due to their nontoxic nature. The present study reports a novel application of the methanolic extract of *Terminalia bellerica* fruits as an environment friendly corrosion inhibitor for steel in sulphuric acid medium. The phytochemicals of the extract, namely Ellagic, Gallic, and Malic acids, play a key role of the anti-corrosive behavior of the extract. The corrosion prevention activity was studied on the steel in 1 M H₂SO₄ using a variety of approaches including weight loss analysis (WL), scanning electron microscope (SEM), electrochemical impedance spectroscopy (EIS), density functional theory (DFT), natural bond orbital analysis (NBO), Fukui function and Monte Carlo simulations (MC). In 1 M H₂SO₄ solution, the maximum electrochemical inhibition efficiency of 91.79% was observed at 4000 mg/L concentration of the extract. The NBO analysis showed that the charge density of the double bonds and the oxygen atoms of carbonyl and hydroxyl groups of the phytochemicals lies on the top of the natural bond orbitals which promotes the anticorrosive properties of the investigated inhibitors. The surface coverage of steel was validated by SEM measurements. According to DFT studies, numerous nucleophilic regions were present in the active phytochemical constituents of the inhibitor, demonstrating their favorable nucleophilicity. The computed electronic structure of the phytochemicals revealed band gaps of 4.813, 5.444, and 7.562 eV for Ellagic, Gallic, and Malic acids respectively suggesting effective metal-inhibitor interactions. A good correlation between experimental and theoretical findings was addressed.

Steel is a preferred choice in variety of industries due to its great mechanical strength. However, in industries, the corrosion of steel occurs because of interaction with corrosive media like sulfuric acid and hydrochloric acid, which are commonly employed for cleaning and descaling purposes¹. Corrosion can cause dangerous and expensive damage to everything from pipelines, bridges, and public buildings to vehicles, water and wastewater systems, and even home appliances². It was indicted the iron rust can easily absorb the Arsenic content and contaminate the external environment³. In addition to the existence of the iron rust can enhance the growth rate of the Legionella bacteria in water. The growth rate can be enhanced by 10³–10⁵ fold with the ferric oxide⁴. The employment of inhibitors is one of the most efficient strategies to inhibit unexpected metal dissolution, particularly in acid solutions⁵. A lot of synthetic chemicals are being used as corrosion inhibitors to reduce corrosion reaction, however many of them have significant environmental consequences and also hazardous to human health⁶. To overcome this problem, natural and biodegradable corrosion inhibitors must be employed

¹Department of Chemistry, College of Science, King Faisal University, Al Ahsa, Saudi Arabia. ²Department of Chemistry, Faculty of Science, Al-Azhar University, Nasr City, Cairo 11884, Egypt. ³Department of Chemistry, Chandigarh University, Mohali, India. ⁴Department of Chemistry, College of Science, University of Bisha, P.O. Box 511, 61922 Bisha, Saudi Arabia. ⁵Department of Chemistry, Government Digvijay Autonomous Postgraduate College, Rajnandgaon, Chhattisgarh 491441, India. ⁶Chemical & Materials Engineering, New Uzbekistan University, 100007 Tashkent, Uzbekistan. ⁷Medical School, Central Asian University, 111221 Tashkent, Uzbekistan. ✉email: aabuelela@kfu.edu.sa; ahmed.abuelela@azhar.edu.eg; akhil.uis@cumail.in; m_bedier@ub.edu.sa

due to their non-toxicity and affordability. Various phytochemicals are present in plant extracts, like terpenoids, alkaloids, flavonoids, coumarins, tannins and poly phenols that contain heteroatoms that effectively play role in protective layer formation on the steel surface⁷⁻⁹. Several plants are available from the literature having different phytochemicals as demonstrated in Table 1¹⁰⁻¹⁷.

The existence of phytochemicals boosts the effectiveness of plant as corrosion inhibitors. Corrosion of steel in aggressive media can be controlled by using such green inhibitors that comprise various heteroatoms like oxygen, nitrogen, and sulfur¹⁸⁻²³.

Bhawsar et al.²⁴ observed that the extract of *Nicotiana tabacum*, which include nicotine, inhibit steel in 2 M sulphuric acid, with efficiency of 94% in 1 g/L. *Rauwolfia macrophylla* was discovered as a corrosion protector in HCl as well as in H₂SO₄ because of the presence of alkaloids perakine and tetrahydroalastone²⁵. These phytochemicals suppress, or even prevent the corrosion of the steel when employed in acidic media. Numerous plant parts, having different phytochemicals were used as corrosion inhibitors and showed good inhibition efficiency as presented in Table 2²⁶⁻⁴⁰.

The main vision of the current research is to determine the inhibitory effect of fruit extract of *Terminalia bellerica*. This extract can be used as a pickling agent to reduce the corrosion of steel in industries where acid corrosion occurs. *Terminalia bellerica* also known as baheda that is a species of *Combretaceae* and a huge deciduous tree that can be found on the plains and on the lower slopes. Medicinal properties of the *Terminalia bellerica* fruit have been studied earlier; however, anticorrosive properties were not investigated yet. A literature survey reveals that *Terminalia bellerica* extract contains Ellagic, Gallic, and Malic Acid^{41,42} as displayed in Fig. 1. The following study include electrochemical measurements, surface morphology measurements, DFT calculations and Monte Carlo simulations.

Experimental studies

Specimen preparation

The steel alloy composition used in the study is depicted in Table 3. The steel sample has a 1 cm² surface area. Each steel coupon was cleaned using several sandpapers prior to the corrosion examination.

S. No	Plant name	Phytochemicals	References
1	Echinacea root extract	Polysaccharides, caffeic acid derivatives, alkaloids, and lipoproteins	10
2	<i>Papaver somniferum</i>	Narcotine, Papaverine and Thebaine	11
3	<i>Allium sativum</i>	Disulphide	12
4	<i>Sida cordifolia</i>	Vasicinone	13
5	<i>Saraca ashoka</i>	Epicatechin	14
6	<i>Cuscuta reflexa</i>	3-methoxy-3,4,5,7-tetrahydroxy flavones	15
7	<i>Armoracia rusticana</i>	Wine lactone	16
8	<i>Myristica fragrans</i>	Phenolic compound	17

Table 1. Different phytochemicals in plants.

S. no.	Plant name	Plant Part	Efficiency/ Conc. of extract	Medium used	Phytochemicals	Reference
1	<i>Cryptostegia grandiflora</i>	Leaves	87% at 500 ppm	1 M H ₂ SO ₄	Hydroxyl cinnamic acid	26
2	<i>Citrus aurantium</i>	Leaves	89% at 10,000 ppm	1 M H ₂ SO ₄	Phenolic compound	27
3	Chinese gosebery fruit	Fruit shell	92% at 800 ppm	1 M HCl	Sucrose and maltose	28
4	<i>Borage flower</i>	Flower	91% at 800 ppm	1 M HCl	Lactic acid and nicotinic acid	29
5	<i>Parseley petroselinum</i>	Leaves	92% at 5000 ppm	1 M HCl	Chromen-2-one	30
6	<i>Lansea coromandelica</i>	Leaf	93.8% at 2000 ppm	1 M H ₂ SO ₄	Flavonoids	31
7	<i>Aloe Vera</i>	Leaves	96% at 300 ppm	1 M H ₂ SO ₄	Anthrones	32
8	<i>Nauclea latifolia</i>	Root	94% at 4000 ppm	1 M H ₂ SO ₄	Saponins	33
9	<i>Ficus racemose</i>	Stem	90.5% at 2500 ppm	1N H ₂ SO ₄	Triterpenes, sterols, long chain fatty acids	34
10	<i>Cannabis sativa</i>	Leaves	97.31% at 200 ppm	0.5 M H ₂ SO ₄	Cannabinoids	35
11	<i>Hemidesmus indicu</i>	Leaves	98.05 at 4000 ppm	1 M H ₂ SO ₄	Alkaloids, tannins, saponins and steroids	36
12	Coconut	Coir dust	94.3% at 500 ppm	0.5 M H ₂ SO ₄	Saponins, flavonoids, tannins, phlobatannins, polyphenols and anthraquinones	37
13	<i>Adhatoda vasica</i>	Leaves and flower	98.9% at 3000 ppm	0.5 M H ₂ SO ₄	Vasicine and vasicinone	38
14	<i>Citrullus lanatus</i>	Fruit	91% at 800 ppm	1 M HCl	Citrulline and nesperetin	39
15	<i>Eucalyptus</i>	Leaves	88% at 800 ppm	1 M HCl	Eucalyptone and ellagic acid	40

Table 2. Corrosion inhibition efficiency of some plants.

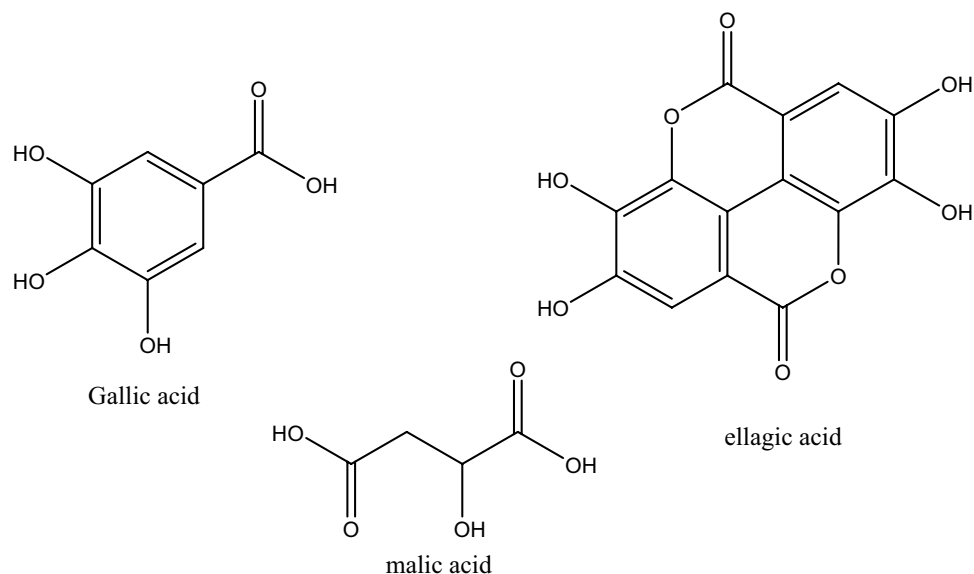


Figure 1. Phytochemicals constituents of *Terminalia bellerica*.

S. no.	Metals present	% composition
1	Iron	99.2
2	Silicon	0.120
3	Carbon	0.105
4	Manganese	0.378
5	Phosphorus	0.079
6	Sulphur	0.0798

Table 3. Composition of the studied steel coupons.

Sample collection and preparation of an inhibitor

Plants (either cultivated or wild), including the collection of plant material, complied with relevant institutional, national, and international guidelines and legislation. *Terminalia bellerica* fruit sample was purchased from the market of Sirhind, Punjab. The dried fruits were then crushed to a powder using a grinder. Then 250 g powdered fruits were refluxed at 50 °C for around 24 h using a Soxhlet apparatus and 250 ml of methanol. A hot water bath was then utilized to dry the extract. The concentration range of the *Terminalia bellerica* fruit extract employed was (1000–4000 mg/l) in 1 M H₂SO₄ solution.

Preparation of the corrosive media

For the current experiment, we utilized a 1 M H₂SO₄ solution that was made using AR grade sulphuric acid from Loba Chemie in double-distilled water. To get various extract concentrations, it was then further diluted.

Weight-loss measurement

Before every corrosion study, the 1 cm² steel coupons were polished with emery paper of various grades. The steel coupons were firstly weighed and then submerged in 1 M sulphuric acid with several inhibitor concentrations (1000, 2000, 3000, and 4000 mgL⁻¹) for 24 h. The coupons of steel were taken out after being exposed to acidic media. Following acetone rinsing and drying of the coupons, the weight loss data were computed using the following equation^{43,44}:

$$\eta\% = \frac{W_0 - W_i}{W_0} \times 100 \quad (1)$$

$$\theta = \frac{W_0 - W_i}{W_0} \quad (2)$$

$W_0 - W_i = \Delta W$ is the weight loss (mg), where w_0 and w_i is the loss of weight without inhibitor and with involvement of inhibitors, respectively and θ is the surface coverage.

Electrochemical studies

Electrochemical analysis (PDP and EIS) of the steel coupons was performed with a Metrohm Autolab electrochemical analyzer^{45,46}. There were three electrodes connected in the corrosion cell: a working electrode made of steel, a reference electrode made of saturated calomel, and a counter electrode made of platinum. The steel was covered with araldite resin, leaving a 1 cm² active region exposed. Current–potential curves were obtained by varying the electrode potential between –250 and +250 mV in relation to the open circuit potential^{45,46}.

The following relationship is used to calculate efficiency⁴⁷:

$$\eta\% = \frac{I_{0corr} - I_{icorr}}{I_{0corr}} \times 100 \quad (3)$$

I_{0corr} and I_{icorr} are measurements of the corrosion current density without and with plant extract. The same electrochemical workstation was employed for PDP analysis as well as for EIS measurements. To set the OCP, the steel electrode was immersed in the acidic medium for approximately 45 min prior to each experiment. The effectiveness of the inhibition was evaluated using the following equation⁴⁸:

$$\eta\% = \frac{R_{ct} - R_{ct}^0}{R_{ct}} \times 100 \quad (4)$$

R_{ct}^0 is used to demonstrate the charge transfer resistance of a solution without any plant extract in it, and R_{ct} that refers to the charge transfer resistance of a solution containing a plant extract.

Phytochemical testing

Methanolic extract of *Terminalia bellerica* was examined for the phytochemicals like alkaloids, flavonoids, saponins, sugar, coumarin, and quinones. A testing solution was prepared by dissolving 0.35 gm of the concentrate in 50 mL of methanol which was subsequently utilized for the phytochemicals investigated. Numerous studies were carried out to assess the phytochemical conformation⁴¹.

UV–visible spectra analysis

Using a UV–Visible spectrophotometer, the spectrum of a *Terminalia bellerica* extract in 1 M H₂SO₄ was determined. To describe the adsorption/desorption behavior of the inhibitor, UV/Visible analysis was conducted for the solutions in which steel specimen was dipped for 24 h and for solutions in which steel specimen was not dipped. To understand the inhibitory mechanism, both spectra was assigned⁴⁹.

Surface inspection

SEM and AFM data of steel were utilized to estimate the surface morphology during the corrosion-protection process. The SEM and AFM pictures of cleaned steel specimen and steel that was dipped in an acid solution without and with an inhibitor were examined.

Theoretical models

Initial guesses of structures of Ellagic, Gallic, and Malic acids were prepared by ChemBioDraw Ultra 14.0 in 2D dimensions then a minimization (energy/geometry) was performed by Gaussian 09 revision-A.02-SMP package⁵⁰ at B3LYP/6-31 g(d,p) level^{51–53}. The optimized parameters were reached after achieving the convergence criteria indicated by Gaussian 09: the maximum remaining force on an atom and the average root mean square (RMS) force on all atoms are below the tolerance threshold 45×10^{-5} and 30×10^{-5} Hartree, respectively as well as the maximum structural drift of one coordinate and RMS change over all structural parameters in the last two iterations are below 18×10^{-4} and 12×10^{-4} Å, respectively. Obtained optimized molecules representing local minima were sketched by Gauss view 6 and presented in Fig. 2⁵⁴.

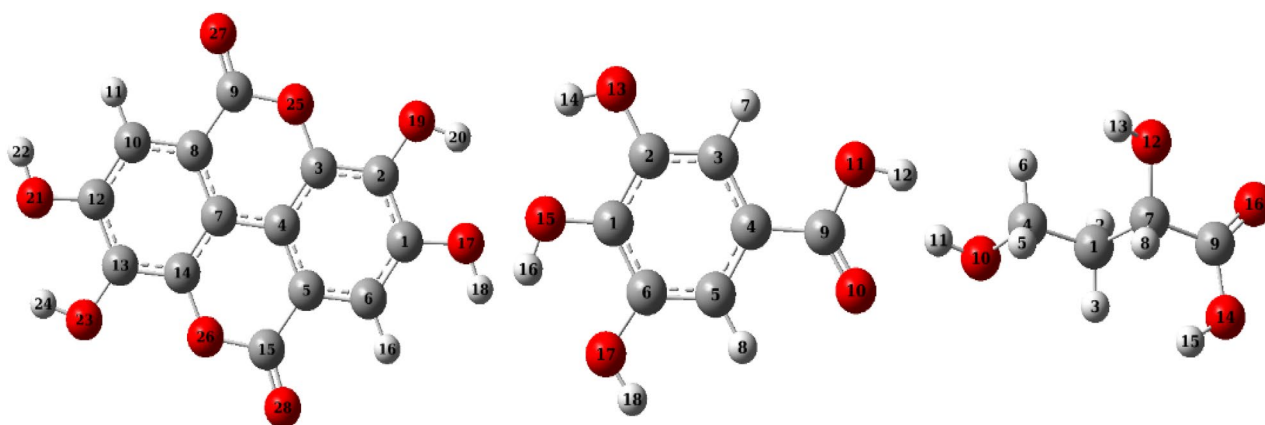


Figure 2. Optimized structural parameters at B3LYP/6-31g(d,p): from left (ellagic, gallic and malic acids).

Often Density Functional Theory (DFT) calculations underestimate Frontier molecular orbitals eigen values⁵⁵, therefore the DFT calculations were repeated using the Time-dependent density-functional theory (TD-DFT) method to calculate the lowest excited state energy and therefore correct the value of band gap energy ΔE_{gap} between Highest Occupied Molecular Orbital (HOMO) and Lowest Unoccupied Molecular Orbital (LUMO). Six energy states were included for this calculation at TD-B3LYP/6-31 g(d,p) following the procedure described by Ref.⁵⁵. E_{HOMO} and E_{LUMO} as well as their corresponding reactivity descriptors were obtained as described by Ref.⁵⁶. HOMO and LUMO surfaces with an iso value of 0.02 and density of 0.0004 were presented as transparent surfaces using the molecular orbital editor of Gauss view 6⁵⁷. Natural bond orbitals (NBOs) were measured at B3LYP/6-31 g(d,p) level for selected sites of Ellagic, Gallic, and Malic acids. NBOs surfaces were created using the NBO Version 3.1⁵⁸ in Gaussian 09 software and plotted using the same isovalue of 0.02 and density of 0.0004 in order to compare them to Frontier Molecular Orbitals (FMOs). In addition, Fukui functions were calculated by addition of a positive and a negative charge to the neutral molecules and then re-optimizing it at B3LYP/6-31g (d,p).

Including water as a solvent, ($2H^+$ and SO_4^{2-}) as corrosive medium (200 H_2O , 20 H_3O^+ , 10 SO_4^{2-}), a Monte Carlo simulation had been used to get deeper details of the adsorption pattern for the *Terminalia bellerica* fruit extract phytochemical structures and their binding with the metal surface. The simulation was done using the Adsorption Locator module included in the Materials Studio 7.0 program⁵⁹. All constituents within the structure were optimized using a COMPASS force field. Fe (1 1 0) unit cell with 11 layers of (11×11) atoms (under periodic boundary conditions with size $18.386 \times 22.341 \times 22.341$ Å) and a vacuum slape of 30 Å which was employed to depict the steel surface. The electrostatic energy was determined using the Ewald summation technique, whereas the van der Waals energy was calculated utilizing the atom-based procedure⁶⁰.

Result and discussions

Measurements of weight reduction

Weight loss values, surface coverage and inhibitory effectiveness were determined and presented in Table 4 at varying concentrations of *Terminalia bellerica* extract at different environment temperatures. According to the information in the Table 4, by raising the extract's concentration, inhibition effectiveness increases (approached a maximum value of 83.38% at 4000 ppm and 298 K) while the corrosion rate decreased, which can also be inferred from the plot in Fig. 3. The corrosion rate was calculated using the following equation⁶¹:

$$\text{Corrosion rate (mpy)} = \frac{kxW}{DxAxT} \quad (5)$$

where K is the corrosion constant, W is the loss of weight after corrosion (mg), A is the total area of the coupon (cm^2), T is the corrosion time (h) and D coupon density (g/cm^3). This increase in inhibition effectiveness is only possible if electron-rich hereto atoms were adsorbed on the steel surface so that it retards the rate of metal corrosion in the abrasive medium^{62,63}.

As the temperature ascending from 298 to 318 K, the rate of corrosion was raised which led to a decline in protection ability (Table 4, Fig. 3). Physical adsorption may be responsible for the decline in protective efficacy with raising temperature at all the evaluated doses. Due to desorption, the inhibitor molecules get detached from the steel substrate at elevated temperatures⁴³.

Adsorption isotherm

The data calculated by weight loss analysis can be fitted to different isotherms to examine the adsorption characteristics⁶⁴. The fitting results were collected for four different isotherms (Freundlich, Langmuir, Temkin and kinetic-thermodynamic models) in Table 5 and Fig. 4. Langmuir model showed high fitting affinity to the

Corrosive medium	Temp (K)	Conc. (mg/L)	Weight loss (mg)	Corrosion rate	Efficiency (%)	Surface coverage (θ)
1 M H_2SO_4	298	0	3.419	390.544	–	–
	298	1000	1.048	119.711	69.34	0.6934
	298	2000	0.714	81.559	79.11	0.7911
	298	3000	0.611	69.793	82.12	0.8212
	298	4000	0.568	64.881	83.38	0.8338
	308	0	5.718	653.153	–	–
	308	1000	2.254	257.469	60.58	0.6058
	308	2000	1.920	219.317	66.42	0.6642
	308	3000	1.624	185.506	71.59	0.7159
	308	4000	1.315	150.209	76.28	0.7628
	318	0	7.824	893.717	–	–
	318	1000	3.365	384.376	56.99	0.5699
	318	2000	3.112	355.476	60.22	0.6022
	318	3000	2.659	303.731	66.01	0.6601
	318	4000	2.365	270.148	69.77	0.6977

Table 4. Weight loss data of inhibition efficiency and surface coverage of *Terminalia bellerica* in 1 M H_2SO_4 .

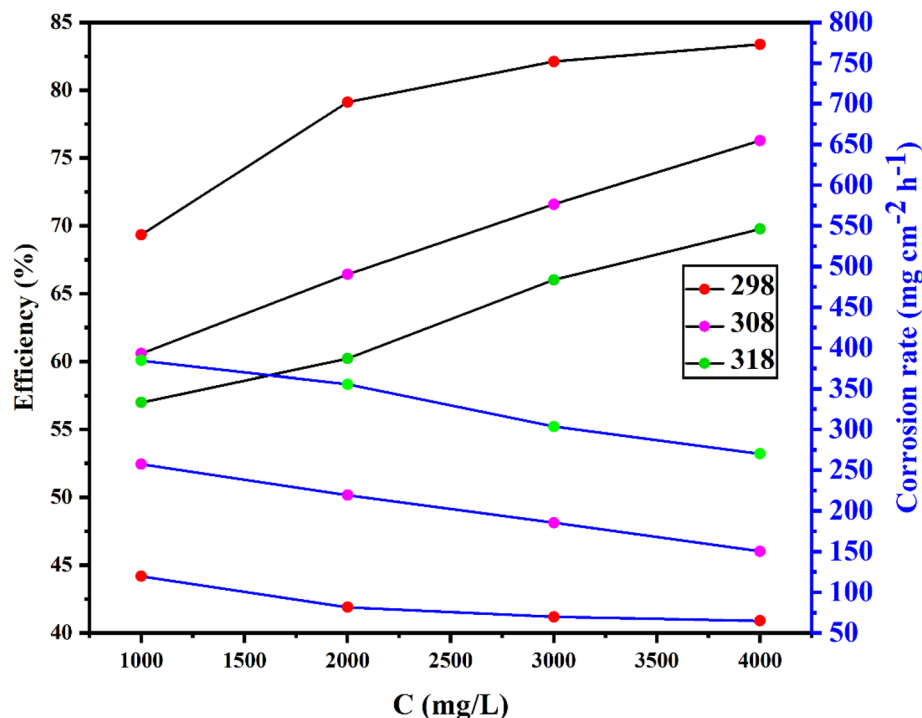


Figure 3. Corrosion inhibition efficiency of *Terminalia bellerica* extract at different concentrations.

Adsorption isotherm model	Linear form equation	Temp (K)	Slope	Intercept	R ²	K _{ads} (ppm ⁻¹)	ΔG ^o _{ads} (kJ/mol)
Freundlich	$\log \theta = \log K + 1/n \log C$	298	0.14	-0.56	0.95	0.28	-31.55
		308	0.16	-0.71	0.99	0.19	-30.67
		318	0.15	-0.69	0.94	0.20	-30.80
Langmuir	$\frac{c}{\theta} = \frac{1}{K} + c$	298	1.12	307.57	1.00	0.00	-20.37
		308	1.20	534.36	1.00	0.00	-18.98
		318	1.32	548.71	1.00	0.00	-18.91
Temkin	$\theta = -\frac{1}{2a} \ln C - \frac{1}{2a} \ln K$	298	9.25	0.45	0.96	1.05	-34.92
		308	8.80	1.66	0.98	1.21	-35.28
		318	10.13	1.29	0.93	1.14	-35.13
Kinetic-thermodynamic	$\log \left(\frac{\theta}{1-\theta} \right) = y \log K + y \log c$	298	0.59	-1.38	0.97	0.00	-21.09
		308	0.52	-1.39	0.96	0.00	-19.29
		318	0.40	-1.09	0.92	0.00	-18.88

Table 5. Adsorption isotherms models of the *Terminalia bellerica* with values of R², slopes, intercepts, and thermodynamic parameters (K_{ads} and ΔG^o_{ads}) by using data obtained from WL measurements.

WL data (R² = 0.99986 at 298 K, 0.99669 at 308 K and 0.99535 at 318 K)⁶⁵. By plotting C/θ vs. log C, Eq. (6) can be employed to calculate the adsorption⁶⁶:

$$\frac{C}{\theta} = \frac{1}{K_{ads}} + C \quad (6)$$

Where surface coverage is represented by θ, inhibitor concentration is depicted by C while K_{ads} is the adsorption equilibrium constant.

The relationship between the concentrations of *Terminalia bellerica* extract and C/θ is depicted in Fig. 4. The resultant plot is linear, and the adsorption equilibrium constant (K_{ads}) can be measured by using the intercept. The corresponding K_{ads} values are 0.0033, 0.0019 and 0.0018 ppm⁻¹ at the temperatures 298 K, 308 K, and 318 K, respectively.

The following formula was used to determine the ΔG^o_{ads} from the K_{ads} values⁶⁷:

$$\Delta G_{ads}^{\circ} = -RT \ln(10^6 \times K_{ads}) \quad (7)$$

Where ΔG^o_{ads} is the standard free energy of adsorption; R is the gas constant; T is the absolute temperature.

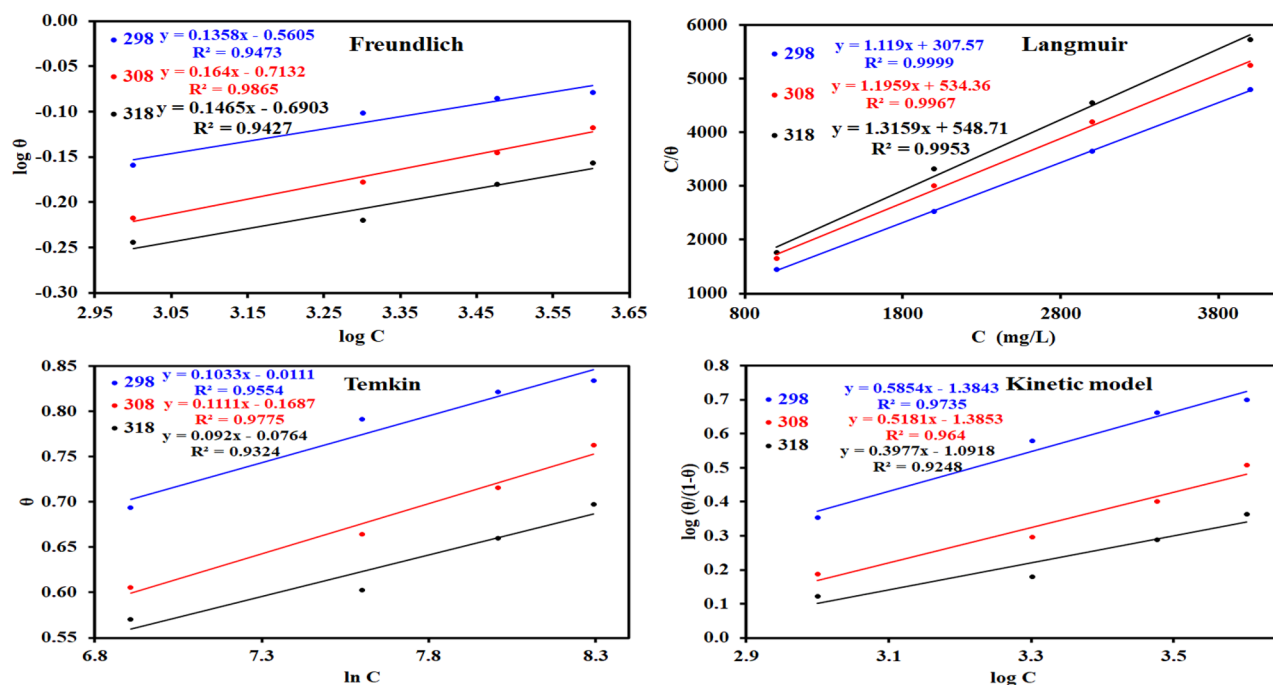


Figure 4. Adsorption isotherms for *Terminalia bellerica* on steel in 1 M H_2SO_4 .

The obtained values of ΔG_{ads}^0 , by using Eq. (7), are -20.37 , -18.98 and -18.91 kJ mol^{-1} at the temperature of 298 K, 308 K, and 318 K, respectively. In general, values of ΔG_{ads}^0 around -20 kJ/mol or more positive are indicative of the inhibitor's physisorption on the surface, likewise, values of -40 kJ/mol or more negative are indicative of the inhibitor's chemisorption on the steel surface⁶⁸. Due to possible interaction between the above-mentioned phytochemicals and the surface of the metal, they can be considered as effective corrosion inhibitor. The inhibitor layer prevents corrosion by obstructing the active sites upon the steel's surface and the physical adsorption is predominant.

Activation parameter

Figure 5a demonstrates a linear relationship between $\ln(CR)$ and $1/T$, from which E_a can be figured out. Using Eq. (8), E_a can be calculated and with accordance to the Arrhenius law, E_a varies as temperature rises, which accelerates metal corrosion.

$$E_a = -\text{Slope} \times 8.314 \quad (8)$$

When an inhibitor was added, E_a (Table 6) was increased from 32.69 to 58.19 kJ/mol , demonstrating the physical adsorption of the inhibitor onto the metal surface⁶⁹. Due to the development of a protective layer over the exposed steel surface, activation energy has therefore increased, suggesting that dissolved steel has been reduced.

Adsorption parameter for entropy and enthalpy

The following equation has been used to evaluate the entropy and enthalpy of adsorption:

$$\ln\left\{\frac{CR}{T}\right\} = \log\left\{\frac{R}{N_a h}\right\} + \frac{\Delta S_a}{R} - \frac{\Delta H_a}{RT} \quad (9)$$

In this formula, N_a , h , ΔH_a , and ΔS_a are Avogadro's number, Planck constant, standard activation enthalpy and standard activation entropy, respectively.

By using graph $\ln(CR/T)$ versus $1/T$, as shown in Fig. 5b, the ΔH_a and ΔS_a parameters have been determined and illustrated in Table 6. It can be inferred, the metal is very well protected because a corrosion-preventing energy barrier is maintained, as demonstrated by the fact that H_a is greater when there an inhibitor used (54.46 kJ/mol) compared to solution without inhibitor (29.50 kJ/mol). The inhibitor adsorption leads to a rise in the corrosion reaction's enthalpy (+ve, endothermic). The introduction of the inhibitor produced an entropy value of -21.02 J/mol/K as opposed to the blank solution having entropy of -93.96 J/mol/K .

Electrochemical studies

Potentiodynamic polarization (PDP) study

In the corrosive solvent with various extract concentrations, Fig. 6 clearly demonstrates the anodic and cathodic polarization responses of steel coupons, while Table 7 enlists the related corrosion outcomes and inhibition efficiencies.

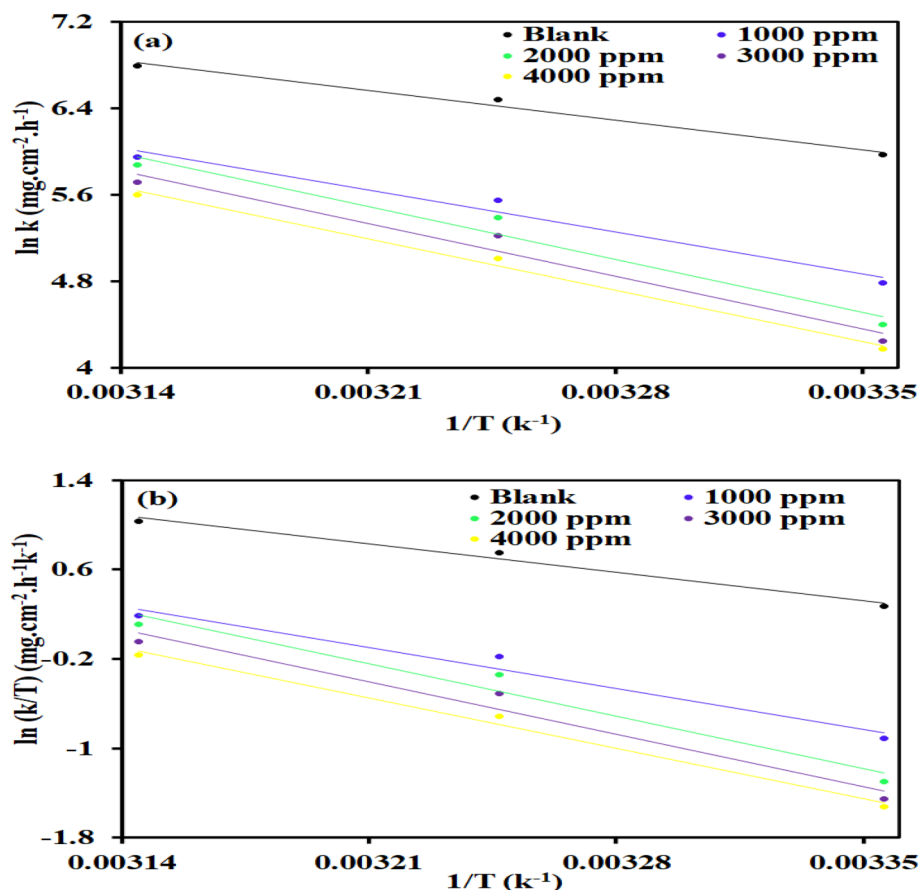


Figure 5. Arrhenius plots and Transition state plots for steel dissolution with and without different concentrations of *Terminalia bellerica* in 1.0 M H₂SO₄ solution.

Inhibitor	Conc. of inhibitor (ppm)	E _a (kJ/mol)	ΔH* (kJ/mol)	ΔS* (J mol/K)
Blank	0.00	32.69	29.50	-93.96
<i>Terminalia bellerica</i>	1000	46.09	42.62	-58.59
	2000	58.19	54.46	-21.02
	3000	58.12	54.40	-22.58
	4000	56.28	52.60	-29.67

Table 6. Activation parameters of dissolution reaction of steel in 1 M H₂SO₄ with at different concentrations of *Terminalia bellerica*.

According to the Tafel curves, the anodic and cathodic section current density is decreasing in the presence of the *Terminalia bellerica* extract. This behavior demonstrate that the inhibitor has the ability to suppress the cathodic hydrogen evolution as well as anodic metal oxidation⁷⁰. The anodic as well as cathodic Tafel graphs (β_a and β_c) with the *Terminalia bellerica* extract has been changed with certain concentrations which show that the inhibitor affects the cathode hydrogen gas evolution and also interfering with the anode iron dissolving process⁷¹. Thus, in a solution of 1 M H₂SO₄, the *Terminalia bellerica* extract regulates both cathodic and anodic corrosion reactions^{72,73}. This should indicate that adding more *Terminalia bellerica* extract prevents the steel corrosion process. According to Table 7, the corrosion current density reduces as *Terminalia bellerica* extract concentration increases⁷⁴. At a concentration of 4000 mg/L, the lowest corrosion current density is 2.610⁻⁴ A/cm² and the best inhibition efficiency showed 91.03%. In addition, Table 7 demonstrates a decline in the corrosion rate in the presence of extract; all this is due to the adsorption capacity of the extract on the surface of the metal which provides remarkable resistance against metal dissolution.

Electrochemical impedance spectroscopy

The resulting Nyquist as well as Bode diagrams are displayed in Fig. 7a, b, and resulted findings are shown in Table 8. Figure 7a also, shows the circuit which was employed in this study.

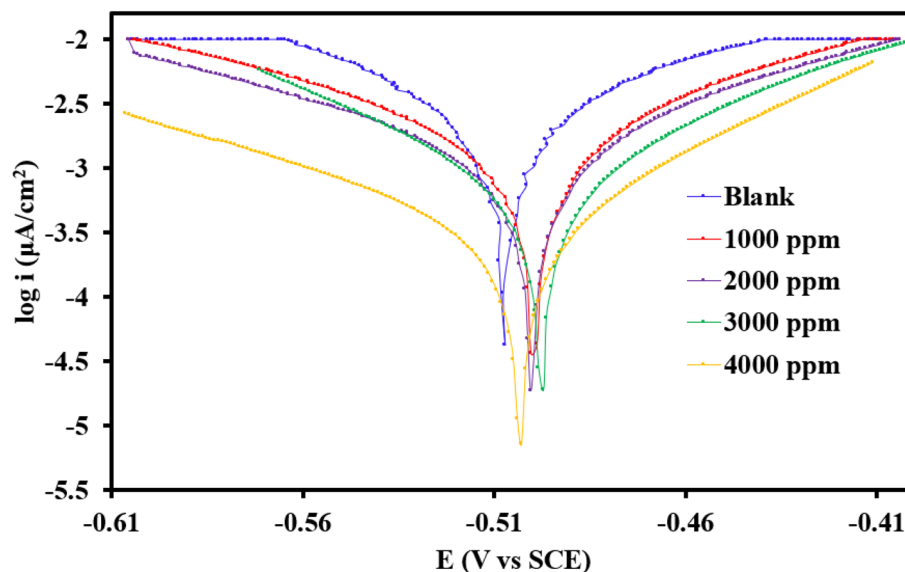


Figure 6. Tafel polarization curves in 1 M H₂SO₄ without and with various concentrations of *Terminalia bellerica* extract.

Inhibitor concentration (mg/L)	E_{corr} (V vs. SCE)	I_{corr} (A cm ⁻²)	β_a (V/dec)	β_c (V/dec)	CR (mpy)	Efficiency (η %)
0	-0.506	2.9×10^{-3}	0.09527	0.06263	34.03	0
1000	-0.480	1.2×10^{-3}	0.1093	0.1204	14.52	58.62
2000	-0.598	1.0×10^{-3}	0.0407	0.03828	12.15	65.51
3000	-0.427	3.4×10^{-4}	0.04677	0.03600	04.23	88.27
4000	-0.523	2.6×10^{-4}	0.07052	0.10421	02.92	91.03

Table 7. Potentiodynamic polarization parameters for steel dissolution without and with various concentrations of extract.

From Fig. 7a, the diameter of the capacitive loops increased when the extract was added compared to that one without extract, indicating that this additive significantly slowed down the dissolution of steel^{75,76}. The profiles of the spectra seem similar, and the semicircular form suggests that the corrosion mechanism was not affected by the presence or absence of the plant extract⁷⁷. The outcomes of Table 8 indicate that increasing the inhibitor concentration while it reaches the highest efficiency at 4000 ppm increases the value of charge transfer resistance and inhibition efficiency. According to the Bode angle diagram, just after introduction of the inhibitor, the establishment of a protective layer on the surface, causes the curves to widen while moving to the left (toward smaller frequencies). In this study, R_{ct} values increase with rise in inhibitor concentrations, which indicates that the extract from *Terminalia bellerica* is easily absorbable on the steel's surface, with a highest efficiency of 91.95% at a concentration of 4000 mg/L being observed. A presence of non-ideal capacitor can be indicated by the slightly flattened semi-circles that result from the electrode flaws and/or surface reactions⁷⁸. In an analogous circuit, the capacitive element's variations are represented by a constant phase element (CPE). The variation of the capacitor behavior for a CPE is represented by a value of $0 < n < 1$ ($n = 1$ represents a pure capacitor)^{72,73}. For n , a value of around 0.8 was found in this study as shown in Table 8.

Analysis of phytochemicals

The phytochemicals found in the *Terminalia bellerica* extract are further described in Table 9.

Test for alkaloids

Wagner's test

The extract was treated with Wagner's reagent. The development of a brownish-reddish precipitate hints the presence of alkaloids⁷⁹.

Mayer's test

Solution was tested for alkaloids using Mayer's reagent. Presence of alkaloids revealed by yellow color in the solution⁷⁹.

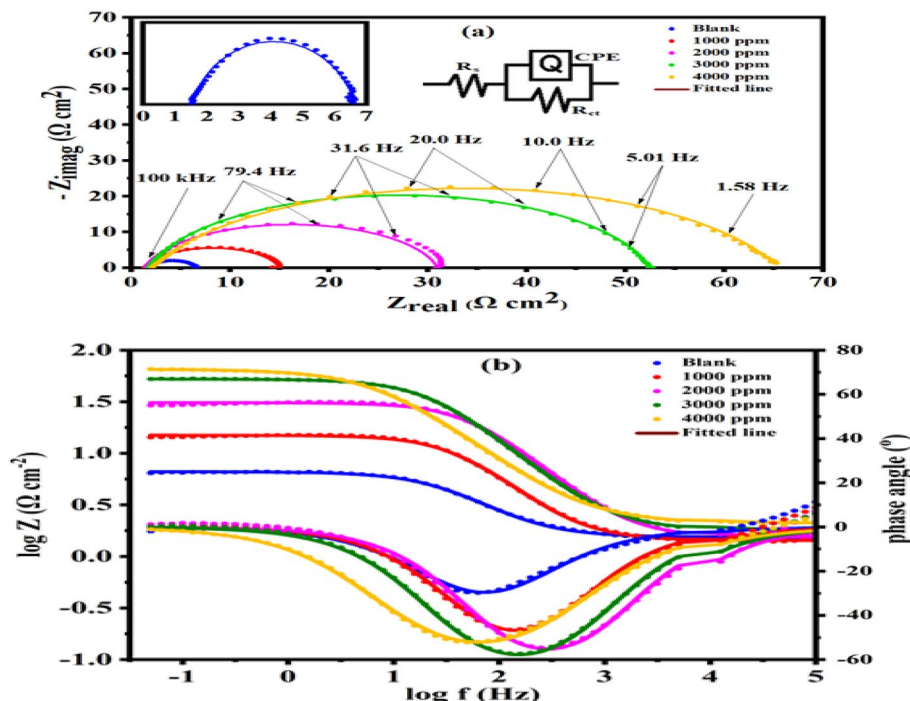


Figure 7. Nyquist (a) and Bode plots (b), and equivalent circuit of constant phase element (CPE) for steel in 1 M H₂SO₄ without and with various concentrations of *Terminalia bellerica* extract at 298 K.

Inhibitor	Conc (ppm)	R _s (Ω cm ²)	R _{ct} (Ω cm ²)	Y ₀ (μ/Ω s ⁿ /cm ²)	n	C _{dl} (μF/cm ²)	Chi squared (χ ²)	S	α°	θ	η _i (%)
Blank	–	1.533	5.109	1500.00	0.822	522.366	2.56 × 10 ⁻³	-0.308	-29.76	–	–
<i>Terminalia bellerica</i>	1000	1.423	13.55	340.90	0.8741	157.125	2.21 × 10 ⁻³	-0.449	-46.52	0.623	62.30
	2000	1.531	29.46	116.30	0.8772	52.538	2.47 × 10 ⁻³	-0.421	-54.60	0.827	82.66
	3000	1.803	50.69	157.30	0.8618	72.483	1.21 × 10 ⁻³	-0.561	-57.40	0.899	89.92
	4000	2.092	63.45	473.40	0.7789	175.023	9.56 × 10 ⁻⁴	-0.573	-52.17	0.919	91.95

Table 8. Electrochemical parameters calculated from EIS measurements on mild steel electrode in 1.0 M H₂SO₄ solutions without and with various concentrations of *Terminalia bellerica* at 298 K. R_s solution resistance, R_{ct} charge transfer resistant, Y₀, n constants of phase elements, C_{dl} double layer capacitance, S slopes of the Bode impedance magnitude at intermediate frequencies, α° maximum phase angle values, θ surface coverage, η_i inhibition efficiency.

S. no	Phytochemicals	Test	Result
1	Alkaloids	Wagner’s test	--
		Mayer’s Test	--
2	Flavanoids	Conc. hydrochloric acid test	++
3	Saponins	Froth test	--
4	Quinones	Concentrated sulphuric acid test	++
5	Coumarins	Alcoholic NaOH test	--
6	Sugar	Fehling solution test	++

Table 9. Phytochemical analysis of *Terminalia bellerica* extract.

Test for flavonoids

After addition of several drops of concentrated HCl to a small amount of the plant extract solution the quick appearance of red color was used to identify the flavonoids⁸⁰.

Test for saponins

Five milliliters of water and five milliliters of filtrate are mixed vigorously. The development of steady foam is a clue that saponins are present.⁸¹

Test for quinones

Upon addition of one mL of the extract in H_2SO_4 , a color change is observed accordingly the existence of quinones is verified.⁸²

Test for coumarin

To about 2 ml of the extract, a few drops of an alcoholic NaOH solution were added. The appearance of a yellow color is an evidence that coumarin exists.⁸²

Test for sugars

Fehling solution test for sugars

Both the Fehling solutions A and B were combined in a one-to-one ratio and then boiled for 1 min. About 1 ml of an extract was taken from that mixture and then heated for 5 to 10 min in the water bath. When yellowish or brick red precipitates first appeared, The presence of carbohydrates is confirmed^{79,80}.

UV visible spectroscopy

UV spectra of *Terminalia bellerica* extracts were analyzed before and after corrosion. The acidic medium having an inhibitor, while the steel was not yet submerged, showed a significantly high absorbance, as shown by the spectra. This was compared to that of the abrasive medium in which the steel was submerged for 24 h, as shown in Fig. 8. When the steel specimen was soaked in the corrosive media containing an inhibitor, a complex between the surface of the steel and the inhibitor was formed. It is clear that the various phytochemicals of the inhibitor have formed a protective layer after being adsorbed to the metal.⁸³

Surface investigation

Scanning electron microscope (SEM)

The morphological changes to the cleaned steel surfaces after a 24-h immersion in 1M H_2SO_4 with or without extract are illustrated in Fig. 9. It can be observed from Fig. 9a that the polished metal surface was not homogeneous and had a few flaws that might serve as corrosion points. Figure 9b shows a very rough surface caused by the rapid and powerful corrosion processes that took place during the immersion of steel in blank H_2SO_4 . Accordingly a protective layer on the steel's surface was created by adding an inhibitor to 1 M H_2SO_4 , thereby reducing the extent of surface damage caused by corrosion (see Fig. 9c)⁸⁴.

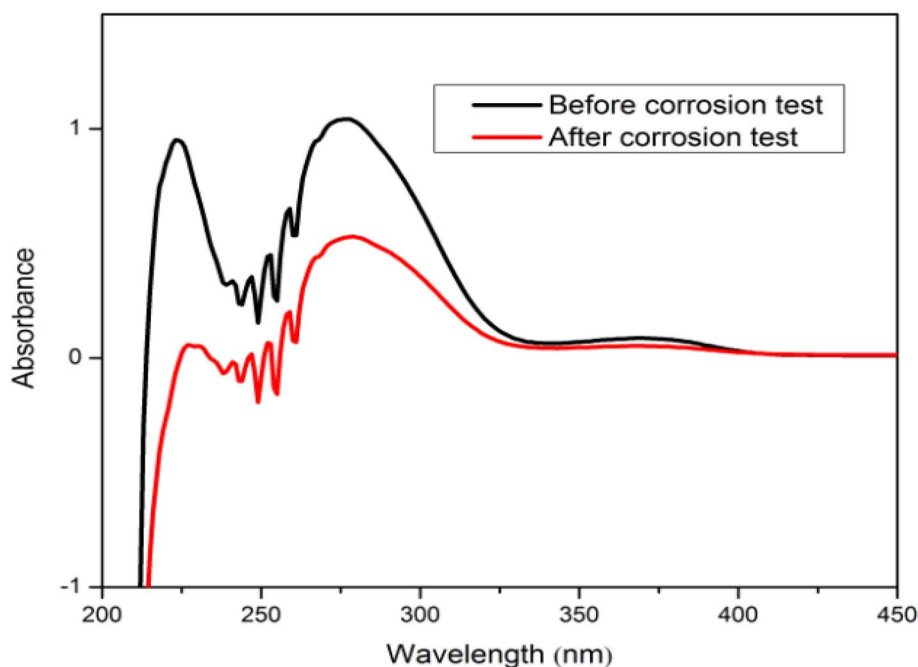


Figure 8. UV spectrum of *Terminalia bellerica* extract before and after the corrosion inhibition performance.

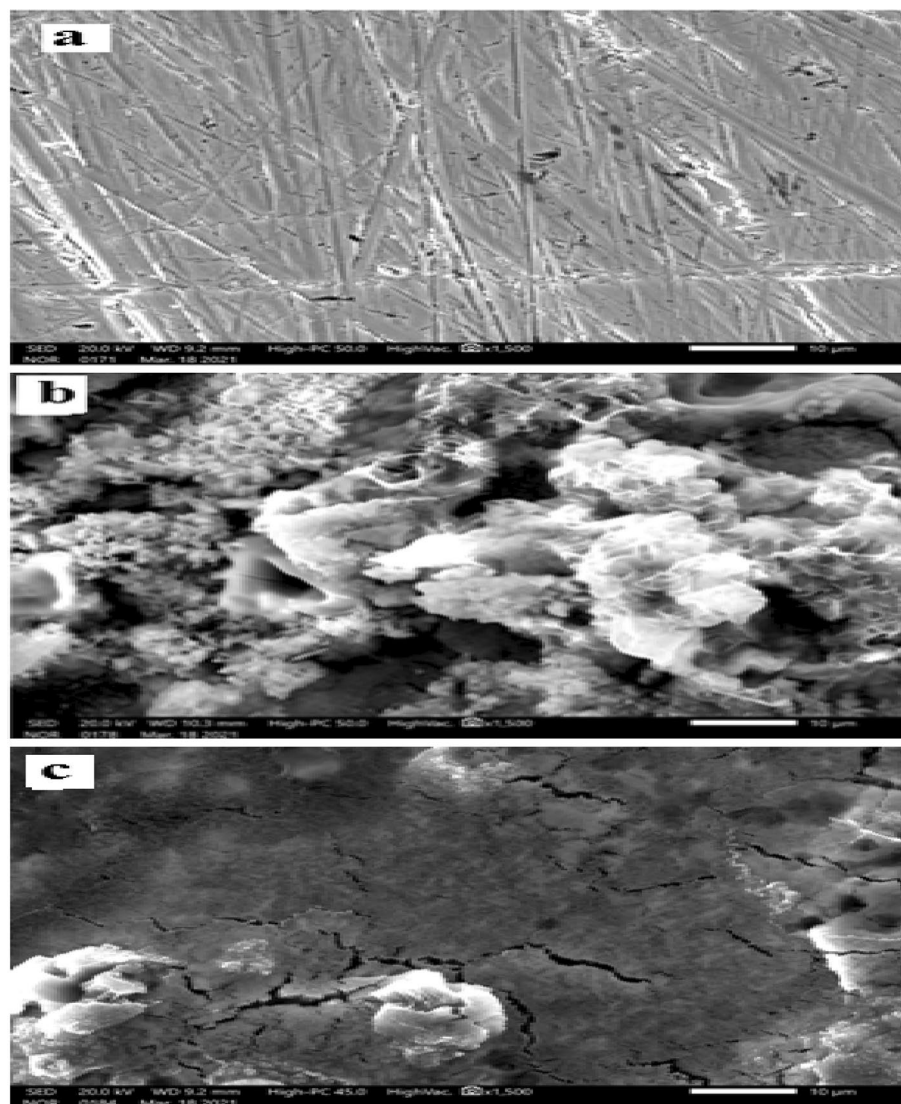


Figure 9. Surface pictures of (a) cleaned mild steel (b) corroded in 1 M H₂SO₄, and (c) inhibited by 4000 mg/L *Terminalia bellerica*'s fruit extract.

Analysis by atomic force microscope (AFM)

Figure 10a–c described the two-dimensional AFM pictures of polished, uninhibited, and protected steel in 1 M H₂SO₄ with *Terminalia bellerica* extract, respectively. For polished steel, the surface roughness value is 2.08 nm. The upper surface of the steel was extensively corroded in the absence of *Terminalia bellerica* extract because steel was dissolved in the acidic solution and the average surface roughness in this condition was 145.75 nm. The surface roughness measured in the presence of *Terminalia bellerica* extract was 23.27 nm. From the values of roughness, it is evident that a protective layer was developed on the metal's surface⁸⁵.

Molecular reactivity

Global reactivity

Organic molecules usually show good reactivity toward metallic surfaces or metal ions because they are rich in π -electrons and lone pairs of hetero atoms⁸⁶. Such loosely tight electrons with low ionization potentials are easily reallocated in the vicinity of d-orbitals of common transition metals^{87,88}. This donating behavior of organic molecules can be evaluated by calculating the global reactivity descriptors including ionization potential, electronegativity, chemical hardness, electron affinity etc. (Table 10) in addition to the band gap between the HOMO and LUMO (Fig. 11). However, the B3LYP method underestimates the HOMO eigen value by average absolute error of 3.10 eV according to Zhang and Musgrave et. al.⁵⁵.

Although it cannot be predicted about the LUMO eigen value that agrees with the recorded electron affinities; therefore, a calculated accurate band gap is a challenge. Nevertheless, the estimated band gap using time-dependent (TD) B3LYP is fairly accurate. Therefore, a correction to the eigen value of HOMO could be used with the TD band gap for accurate estimation of LUMO and hence an accurate prediction for the reactivity descriptors.

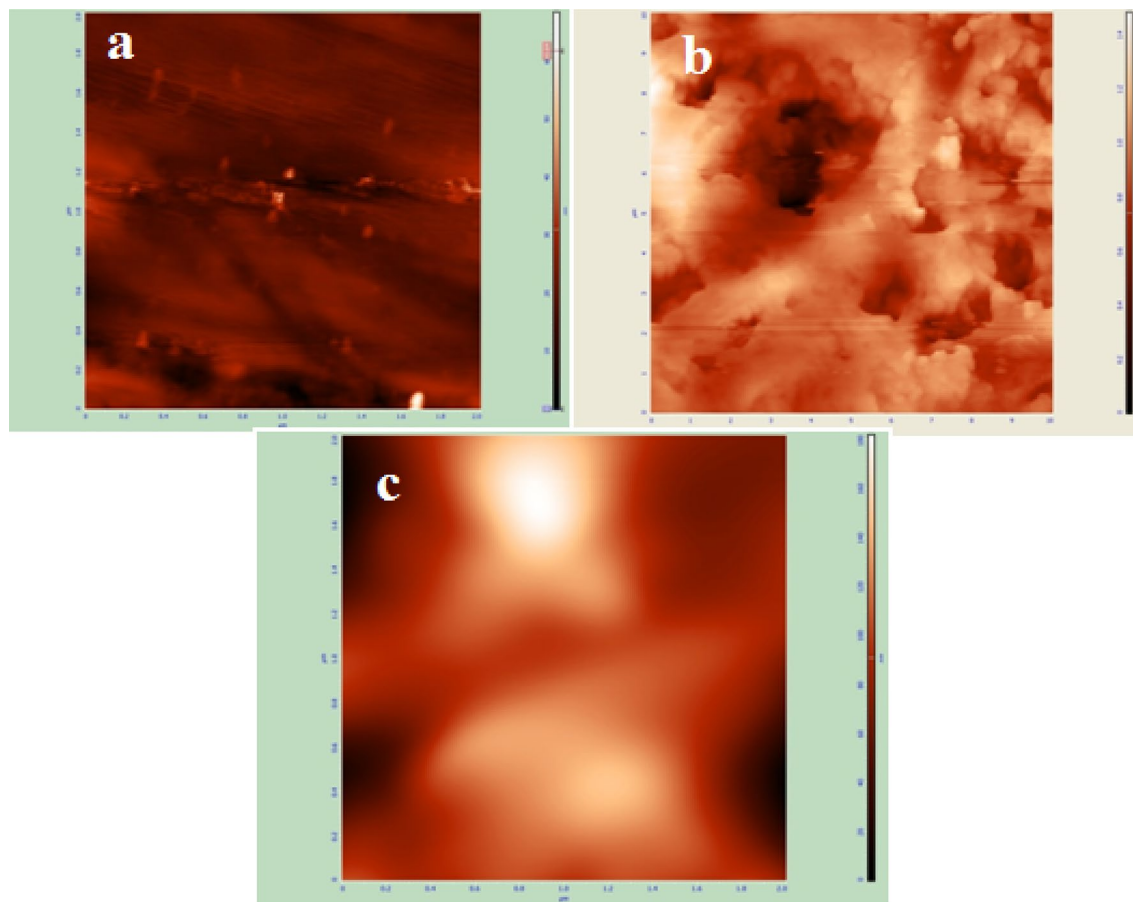


Figure 10. AFM images of (a) cleaned mild steel (b) corroded in 1 M H₂SO₄, and (c) inhibited by 4000 mg/L *Terminalia bellerica*'s fruit extract.

Molecular parameters ^a		Ellagic		Gallic		Malic	
		B3LYP	TD-B3LYP ^b	B3LYP	TD-B3LYP ^b	B3LYP	TD-B3LYP ^b
E _{LUMO}	–	–1.847	–3.91	–1.056	–3.158	–0.232	–2.657
E _{HOMO}	–	–6.086	–8.723	–5.986	–8.603	–7.333	–10.219
ΔE (E _{LUMO} – E _{HOMO})	(E _{LUMO} – E _{HOMO})	4.239	4.813	4.930	5.444	7.101	7.562
Ionization potential (IP)	–E _{HOMO}	6.086	8.723	5.986	8.603	7.333	10.219
Electron affinity (EA)	–E _{LUMO}	1.847	3.91	1.056	3.158	0.232	2.657
Electronegativity (χ)	(IP + EA)/2	3.967	6.317	3.521	5.881	3.55	6.438
Chemical potential (μ)	–χ	–3.967	–6.317	–3.521	–5.881	–3.55	–6.438
Chemical hardness (η)	(IP – EA)/2	2.12	2.407	2.465	2.723	3.782	3.781
Chemical softness (σ)	1/η	0.472	0.415	0.406	0.367	0.264	0.264
Global electrophilicity (ω)	χ ² /2η	3.712	8.289	2.515	6.351	1.666	5.417
ΔN	(χ _{metal} – χ _{inh})/2(η _{metal} + η _{inh})	0.500	0.288	0.508	0.308	0.418	0.228

Table 10. Calculated electronic reactivity indices for ellagic, gallic and malic acids. ^aAll parameters in eV except ΔN is dimensionless quantity. ^bAll values are corrected according to the procedure in Ref.⁵⁵.

Correction of HOMO eigen value is carried out using the formula: $-HOMO_{corr} = A + B(-HOMO_{cal})$ where $A = 1.42$ and $B = 1.20$; correlation parameters of B3LYP functional⁵⁵. Then, an accurate value of LUMO is obtained using the formula: $LUMO = HOMO + \Delta E_{gap}$. The band gap ΔE_{gap} calculated by TD-B3LYP for Ellagic, Gallic and Malic acids are 4.813, 5.444 and 7.562 eV, respectively (Table 10 and Fig. 11). Because the HOMO and LUMO wave functions of a moderate-sized band gap are easily combined, the molecule is quickly polarized and requires less energy to be excited^{56,89}. Therefore, the calculated low energy gaps promote the reactivity of these molecules toward the metal surface and hence their ability as corrosion inhibition candidates in the following order Ellagic > Gallic > Malic acid.

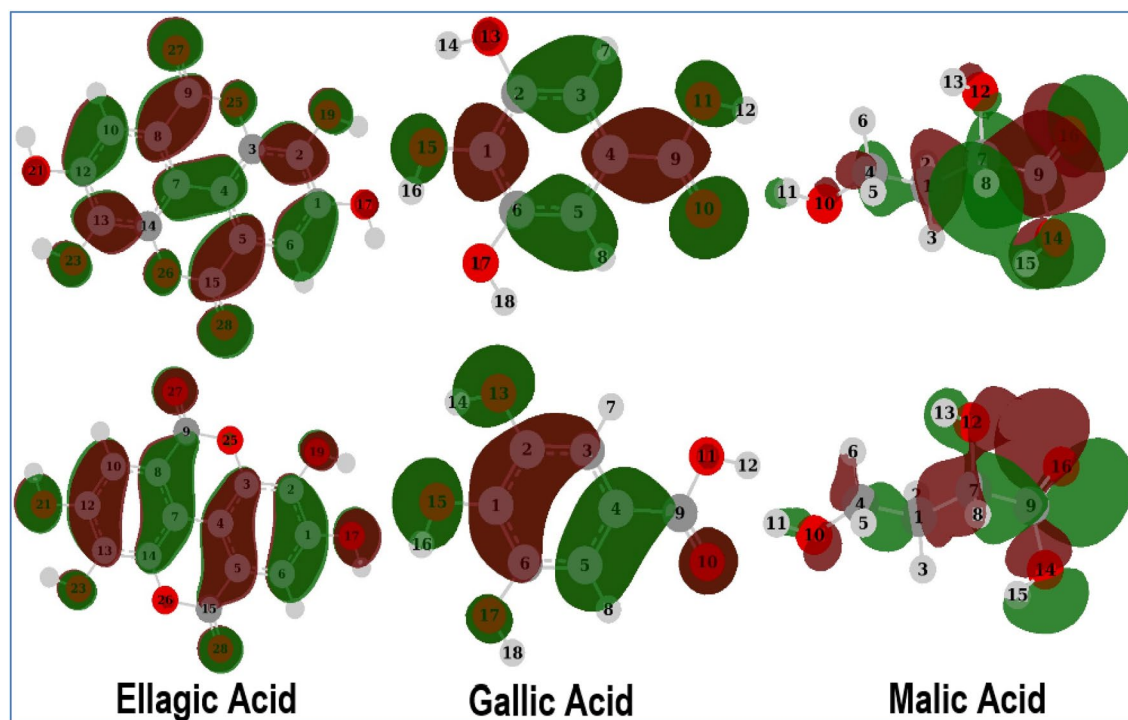


Figure 11. Frontier molecular orbitals: LUMOs (upper row) and HOMOs (lower row).

The calculated eigenvalues for HOMO of Ellagic, Gallic, and Malic acid molecules are -8.723 , -8.603 , and -10.219 eV, respectively (Table 10). These low orbitals eigen values indicate that the electrons occupying these orbitals need few electron volts of energy to be ionized (i.e.: $+8.723$, $+8.603$, and $+10.219$ eV for Ellagic, Gallic, and Malic acid, respectively) and hence can be easily shared into the metal surface. As expected, the HOMOs are mainly localized on the π -system of the carbonyl group and phenyl ring in both Ellagic and Gallic acids and on the carbonyl group and bonds including covalently attached oxygen atoms (Fig. 11). Moreover, the chemical hardness for the studied molecules was estimated as suggested by R. G. Pearson in “chemical hardness”⁵⁶. Pearson suggested that in molecules where the HOMO is filled with electrons, the electronegativity divides the band gap into two parts and the addition of these parts gives the chemical hardness. Having low chemical hardness 2.407, 2.723, and 3.781 (Table 10) for Ellagic, Gallic, and Malic acid, respectively indicates that they are good candidates for strong and efficient interactions with the metal surface. Furthermore, the mutual tendency of charge transfer between two interacting entities, in this case, inhibitor and metal surface, could be calculated as follows⁹⁰:

$$\Delta N = \frac{(\chi_{metal} - \chi_{inh.})}{2(\eta_{metal} + \eta_{inh.})} \quad (10)$$

where χ and η are electronegativity and chemical hardness, respectively. The predicted ΔN for the Ellagic, Gallic, and Malic acid are 0.288, 0.308, and 0.228, respectively (Table 10) revealing the good tendency of these molecules to mutually share electrons with the metal surface. Overall, global reactivity indices suggest a feasible mutual inhibitor-metal interactions between Ellagic, Gallic, and Malic acid and mild steel nominating them for effective corrosion suppression and explaining their recorded electrochemical high inhibition efficiency.

Natural bond orbital analysis

The results of NBO analysis are summarized in Tables 11, 12 and 13 for molecules of Ellagic, Gallic, and Malic acid, respectively.

The Tables list natural bond orbitals at expected inhibitor-metal interactions in descending order according to their energies along with their type of bonding, electron occupancy, energy, hybridization, and percent of s and p characters. Moreover, the surface densities of these orbitals are plotted in Table S1 to Table S3 with the same descending order. Analyzing NBOs allows us to determine the importance of individual sites of a molecule to come into interaction with the steel surface. In other words, NBOs order is an order of donating ability of the electron density involved in an interaction. The results in Table 11 show that the electron density of Ellagic acid molecule can be shared into the metal surface in the following order: $LP(2)O_{27} > LP(2)O_{28} > BD(2)C_7-C_8 > BD(2)C_4-C_5 > BD(2)C_{10}-C_{12} > BD(2)C_1-C_6 > BD(2)C_{13}-C_{14} > BD(2)C_2-C_3 > LP(2)O_{23} > LP(2)O_{19} > LP(2)O_{26} > LP(2)O_{25} > LP(2)O_{21} > LP(2)O_{17} > BD(2)C_9-O_{27} > BD(2)C_{15}-O_{28}$. The plots in (Table S1 to S3) show the source orbitals for these NBOs; for example, bonding orbital $LP(2)O_{27}$ originates from HOMO of the Ellagic acid molecule. In other words, the HOMO of the Ellagic acid molecule is localized on the lone pair of the O_{27} atom and it is easier to interact with the steel surface than the other NBOs. In this order, the electronic density of $BD(2)C_{15}-O_{28}$ orbital of the double bond $C_{15}-O_{28}$ comes late at HOMO-15 which indicates a weaker ability to reallocate its density

Type*	Occupancy	Energy	NBO	s % (atom 1)	p % (atom 1)	s % (atom 1)	p % (atom 2)
LP(2)O ₂₇	1.82835	-0.25629	p ^{1.00}	0.11	99.62	-	-
LP(2)O ₂₈	1.82835	-0.25629	p ^{1.00}	0.11	99.62	-	-
BD(2)C ₇ -C ₈	1.63250	-0.27030	0.6930 p + 0.7209 p	0.00	99.98	0.00	99.98
BD(2)C ₄ -C ₅	1.63251	-0.27030	0.6930 p + 0.7209 p	0.00	99.98	0.00	99.98
BD(2)C ₁₀ -C ₁₂	1.69627	-0.28469	0.7068 p + 0.7074 p	0.00	99.95	0.00	99.96
BD(2)C ₁ -C ₆	1.69628	-0.28470	0.7074 p + 0.7068 p	0.00	99.96	0.00	99.95
BD(2)C ₁₃ -C ₁₄	1.63195	-0.28731	0.6970 p + 0.7170 p	0.00	99.95	0.00	99.96
BD(2)C ₂ -C ₃	1.63196	-0.28732	0.6970 p + 0.7170 p	0.00	99.95	0.00	99.96
LP(2)O ₂₃	1.84729	-0.32988	p ^{1.00}	0.00	99.87	-	-
LP(2)O ₁₉	1.84729	-0.32988	p ^{1.00}	0.00	99.87	-	-
LP(2)O ₂₆	1.75054	-0.33587	p ^{1.00}	0.00	99.88	-	-
LP(2)O ₂₅	1.75054	-0.33587	p ^{1.00}	0.00	99.88	-	-
LP(2)O ₂₁	1.88602	-0.33587	p ^{1.00}	0.00	99.90	-	-
LP(2)O ₁₇	1.88602	-0.33587	p ^{1.00}	0.00	99.90	-	-
BD(2)C ₉ -O ₂₇	1.98285	-0.38115	0.5620 p + 0.8271 p	0.00	99.82	0.00	99.66
BD(2)C ₁₅ -O ₂₈	1.98285	-0.38115	0.5620 p + 0.8271 p	0.00	99.82	0.00	99.66

Table 11. Calculated NBOs of ellagic acid at expected adsorption sites. *LP(1): refers to first lone pair, LP(2): second lone pair, etc. BD(1): bonding orbital of a single bond, BD(2): for double bond.

Type*	Occupancy	Energy	NBO	s % (atom 1)	p % (atom 1)	s % (atom 1)	p % (atom 2)
BD(2)C ₃ -C ₄	1.68327	-0.24870	0.6958 p + 0.7182 p	0.00	99.96	-	99.98
LP(2)O ₁₀	1.84659	-0.25446	p ^{1.00}	0.00	99.75	-	-
BD(2)C ₅ -C ₆	1.69592	-0.26659	0.7122 p + 0.7020 p	0.00	99.95	-	99.96
BD(2)C ₁ -C ₂	1.62619	-0.26871	0.7207 p + 0.6933 p	0.00	99.96	-	99.95
LP(2)O ₁₃	1.86908	-0.31224	p ^{1.00}	0.00	99.88	-	-
LP(2)O ₁₁	1.82499	-0.32605	p ^{1.00}	0.00	99.88	-	-
LP(2)O ₁₅	1.87948	-0.33081	p ^{1.00}	0.00	99.90	-	-
LP(2)O ₁₇	1.89289	-0.33607	p ^{1.00}	0.00	99.91	-	-
BD(2)C ₉ -O ₁₀	1.98484	-0.37258	0.5477 p + 0.8367 p	0.00	99.80	-	99.67
BD(1)C ₃ -H ₇	1.97675	-0.51611	0.7970 sp ^{2.26} + 0.6039 s	30.66	69.31	99.95	0.00

Table 12. Calculated NBOs of gallic acid at expected adsorption sites. *LP(1): refers to first lone pair, LP(2): second lone pair, etc. BD(1): bonding orbital of a single bond, BD(2): for double bond.

Type*	Occupancy	Energy	NBO	s % (atom 1)	p % (atom 1)	s % (atom 1)	p % (atom 2)
LP(2)O ₁₆	1.82816	-0.24696	p ^{1.00}	0.01	99.70	-	-
LP(2)O ₁₀	1.95998	-0.30223	p ^{1.00}	0.12	99.79	-	-
LP(2)O ₁₂	1.95228	-0.30692	p ^{1.00}	0.46	99.43	-	-
LP(2)O ₁₄	1.83031	-0.33199	p ^{1.00}	0.01	99.86	-	-
BD(2)C ₉ -O ₁₆	1.99182	-0.38099	0.5689 p + 0.8224 p	0.11	99.71	0.17	99.47
BD(1)C ₁ -H ₂	1.97871	-0.50412	0.7960 p + 0.6053 s	23.67	76.28	99.95	0.00

Table 13. Calculated NBOs of Malic acid at expected adsorption sites. *LP(1): refers to first lone pair, LP(2): second lone pair, etc. BD(1): bonding orbital of a single bond, BD(2): for double bond.

into *d*-orbitals of the steel metal. In accordance, the donating ability of Gallic acid molecule shows the following order: BD(2)C₃-C₄ > LP(2)O₁₀ > BD(2)C₅-C₆ > BD(2)C₁-C₂ > LP(2)O₁₃ > LP(2)O₁₁ > LP(2)O₁₅ > LP(2)O₁₇ > BD(2)C₉-O₁₀ > BD(1)C₃-H₇ as listed in Table 12 while corresponding orbital densities from HOMO-9 are listed in Table S2. Moreover, NBOs of Malic acid show donating behavior following the order: LP(2)O₁₆ > LP(2)O₁₀ > LP(2)O₁₂ > LP(2)O₁₄ > BD(2)C₉-O₁₆ > BD(1)C₁-H₂. It is worth noticing that the number of donating sites follows the order Ellagic > Gallic > Malic which in turn favors the adhering of metal surface in the same order.

Local reactivity

While global reactivity explores the tendency of a molecular entity to be involved in chemical change, local reactivity figures out the sites within this entity to react with another one. For a molecule contacting metal surface and suppress corrosion reaction, it is worthy to have electron rich regions more than electron-poor ones. These regions could be explored using a calculated molecular electrostatic potential (MEP) map shown in Fig. 12.

In such map, electron-rich sites having low electrostatic potential are designated with red color and electron-poor sites are blue colored while sites with green color indicate moderate charge density content. The mapped surfaces presented in Fig. 12 show that the distribution of the colors follows the order: green > blue > red. The existence of wide areas with moderate electron density is common in organic molecules; however, maps of Ellagic, Gallic, and Malic molecules are characterized by electron-rich regions much more than electron poor-regions. The red regions are localized around carbonyl groups which agree with the order of the NBOs where HOMOs are corresponding to the lone pairs of oxygen atoms of the carbonyl groups suggesting that these groups have the priority to contact the metal surface.

Although the localization of electronic density over a particular site indicates its tendency to contact metal surface, which is useful, the magnitude of this conduct cannot be estimated from the MEP map. The magnitude of a particular site to be either nucleophile or electrophile could be determined using Fukui functions. In this procedure, the neutral molecule is charged by either a negative or a positive charge than the second derivative of energy is probed, for each atom, with respect to number of electrons and the external potential owing while molecules approaching each other as follows:

$$f(r) = \partial^2 E / \partial N \partial v \quad (11)$$

A good approximation to solve this equation is to use “condensed” Fukui functions on an atom-by-atom basis⁹¹:

$$f_k^- = [q_k(N) - q_k(N - 1)] \quad (12)$$

$$f_k^+ = [q_k(N + 1) - q_k(N)] \quad (13)$$

Where f_k^- and f_k^+ are electrophilic and nucleophilic Fukui indices, respectively and q_k is the atomic charge. We used Hirshfeld charges since it is corrected to bond orders and is much accurate for molecules having single-double bonds in conjugations. We listed the predicted Fukui indices for the Ellagic, Gallic, and Malic molecules in Table 14 according to the descending order of electrophilic Fukui function since it is of more interest for inhibitor-metal interactions.

Some good information can be inferred from Table 14, for example, in Ellagic acid, the oxygen atoms of carbonyl groups carry the highest ($f_k^- = 0.073$) electrophilic Fukui indices (O_{28} and O_{27}) while those of hydroxyl groups carry lower indices ranging between 0.024 and 0.035 and those involved in the carbon skeleton are of the lowest electrophilic sites (Table 14). The same trend applies to oxygen atoms of Gallic acid; however, the presence of conjugation within the carbon rings provides stronger electrophilic sites than those of oxygen atoms. Finally, the Malic acid has the lowest electrophilic Fukui indices, though its carbonyl is much electrophilic than the corresponding carbonyl of Gallic acid which could be attributed to the conjugation of the latter with the phenyl ring.

Monte Carlo simulations

The modeling at the molecular level was done for the adsorption of *Terminalia bellerica* Fruit Extract (Ellagic, Gallic, and Malic acid) on steel (or Fe (1 1 0)) in the gas phase and the aqueous phase. Figure 13 displays the most stable configurations of the adsorbed *Terminalia bellerica* Fruit Extract modeled using MC in the aqueous phase settings. Figure 13 shows the close contact between *Terminalia bellerica* Fruit Extract constituents and the steel surface. This confirms their ability to compete with water and the corrosive ions in adsorption and so enhance protection⁹². It is noteworthy findings of the MC support the DFT investigation, which showed that the Ellagic structure has a high reactivity (completely flat and parallel adsorption) compared to Gallic and Malic acid, which are partially flat adsorbed. This may be used to support the inhibitory performance of the studied structures.

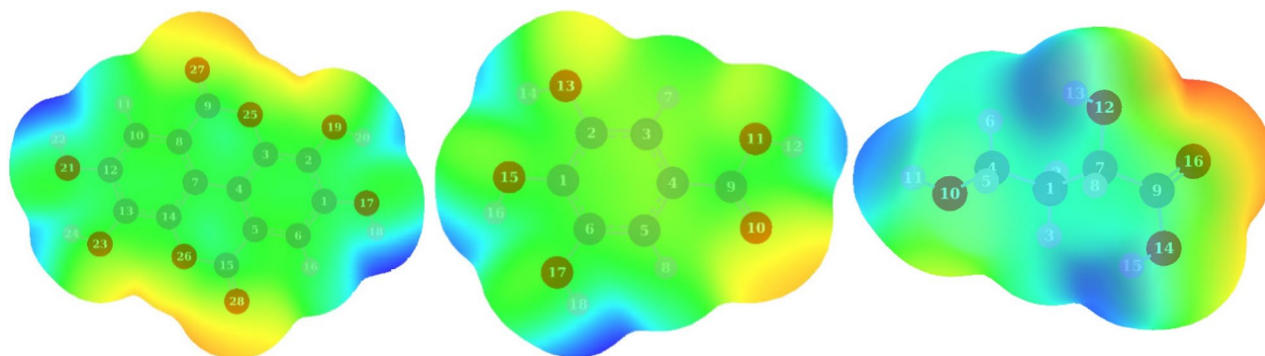


Figure 12. Molecular electrostatic potential (MEP) map: from left (ellagic, gallic and malic acids).

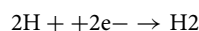
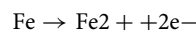
Ellagic			Gallic			Malic		
Atoms	f^+	f^-	Atoms	f^+	f^-	Atoms	f^+	f^-
C ₃	0.018	0.015	O ₁₇	0.430	0.032	C ₁	0.027	0.017
C ₁₄	0.018	0.015	O ₁₃	0.118	0.034	O ₁₂	0.089	0.027
O ₂₅	0.023	0.023	C ₆	0.044	0.042	C ₄	0.048	0.030
O ₂₆	0.023	0.023	C ₂	0.077	0.044	C ₇	0.042	0.038
C ₄	0.032	0.023	O ₁₅	0.116	0.054	O ₁₀	0.152	0.043
C ₇	0.032	0.023	O ₁₁	0.036	0.057	O ₁₄	0.093	0.080
O ₁₇	0.07	0.024	C ₅	0.067	0.062	C ₉	0.069	0.157
O ₂₁	0.07	0.024	C ₄	0.084	0.067	O ₁₆	0.226	0.162
C ₁	0.061	0.032	C ₃	0.040	0.070			
C ₁₂	0.061	0.032	C ₁	0.098	0.084			
O ₁₉	0.05	0.035	C ₉	0.018	0.117			
O ₂₃	0.05	0.035	O ₁₀	0.076	0.122			
C ₆	0.041	0.043						
C ₁₀	0.041	0.043						
C ₅	0.04	0.044						
C ₈	0.04	0.044						
C ₂	0.028	0.054						
C ₁₃	0.028	0.054						
C ₉	0.015	0.055						
C ₁₅	0.015	0.055						
O ₂₇	0.068	0.073						
O ₂₈	0.068	0.073						

Table 14. Calculated condensed Fukui functions for ellagic, gallic and malic acid molecules. Calculated using Hirshfeld charges at B3LYP/6-31G(d,p).

Table 15 displays the binding energy and the different forms of the adsorption energy values for the Ellagic, Gallic, and Malic acid molecules. The spontaneous tendencies of *Terminalia bellerica* Fruit Extract constituents for adsorption are confirmed by negative adsorption energies values⁹³. This is due to the numerous active adsorption sites found on the extract molecules. Based on the binding energy values, Ellagic has the highest binding energy followed by Gallic and Malic acid. This arrangement supports the outcomes of the DFT computation.

Corrosion inhibition mechanism by the extract of *Terminalia bellerica* on steel

A corrosion reaction consists of two electrochemical reactions: oxidation on the anode and reduction on the cathode.



When the electrons of the heteroatoms donate electrons to the empty orbital of the metal, a coordinate bond is formed⁹⁴.

In 1 M sulfuric acid, steel corrosion can be reduced using phytochemicals present in *Terminalia bellerica* extract. These phytochemicals have a variety of functional groups, like carbonyl, hydroxyl, and carboxylic acids, as well as double bonds. Figure 14 illustrates how the lone pair of heteroatoms and the multiple bonds found in the phytochemicals form a coordinate bond. It is the inhibitory activity of the plant extract on the metal surface that leads to blocking of the active site.

Conclusion

1. The weight reduction method, potentiodynamic polarization study, and DFT were used to assess the corrosion resistance of steel immersed in H₂SO₄ in the absence of *Terminalia bellerica* extract and in presence of extract.
2. The addition of a fruit extract from *Terminalia bellerica* seems to increase the effectiveness of corrosion inhibition.
3. It has been found that at a concentration of 4000 ppm, the inhibitory efficacy was 91.79%.
4. The potentiodynamic polarization investigation shows that when the concentration of *Terminalia bellerica* extracts raises, the corrosion current density decreases.
5. The various phytochemicals found in the extract have an impact on the inhibition's potency.
6. As the inhibitor concentration is increased, the inhibition efficiency improves.

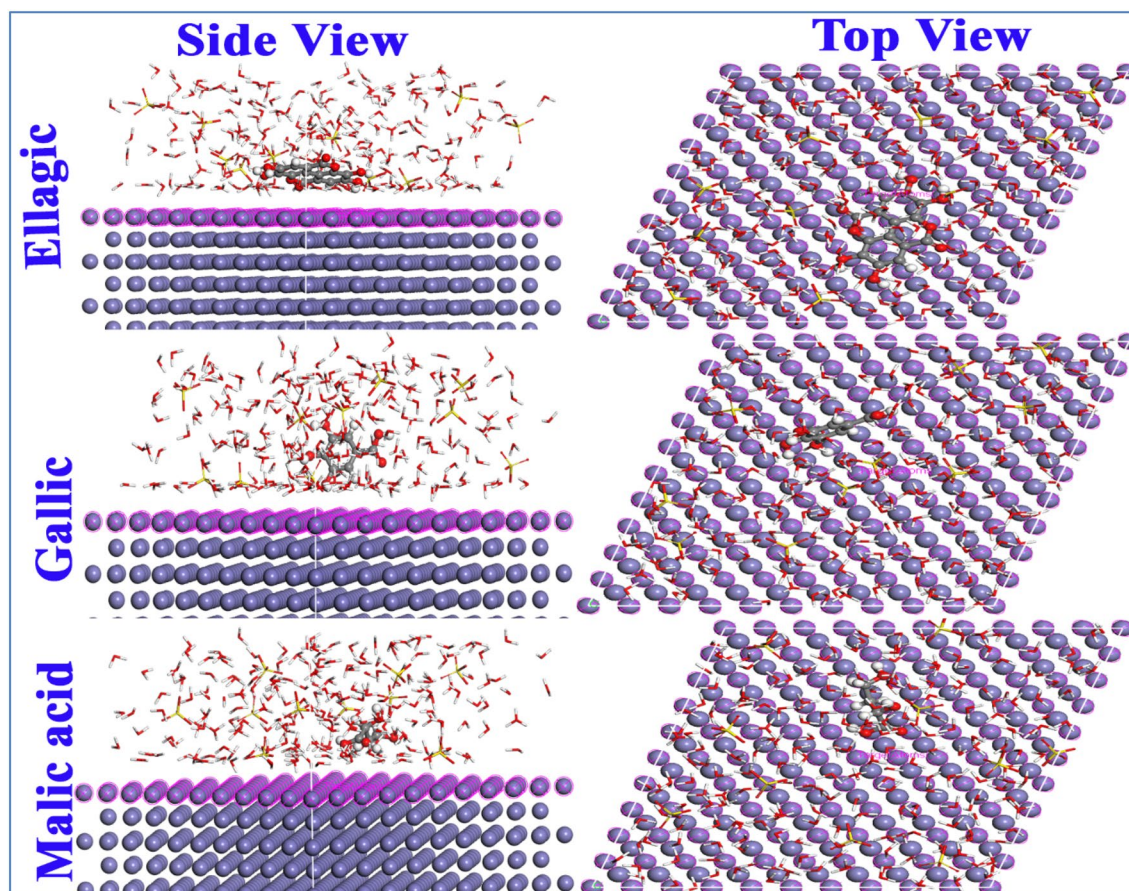


Figure 13. Side and top views of the most appropriate configuration for adsorption of neutral molecules on Fe (110) Surface obtained by MC simulations in the aqueous solution.

Descriptors*	Gas phase			Aqueous phase		
	Ellagic	Gallic	Malic	Ellagic	Gallic	Malic
Total energy	-21.850	-109.310	-62.708	-7765.7	-7794.0	-7626.8
Adsorption energy	-153.146	-88.060	-84.587	-7953.5	-7938.7	-7924.2
Rigid adsorption energy	-146.755	-84.648	-63.882	-8006.1	-7993.3	-7961.6
Deformation energy	-6.390	-3.412	-20.705	52.5	54.5	37.5
($dE_{\text{ads}}/dN_{\text{Fe}}$)	-153.146	-88.061	-84.587	-127.2	-81.8	-65.1
Binding energy	153.146	88.061	84.587	7953.5	7938.7	7924.2

Table 15. The outputs and descriptors calculated by the Monte Carlo simulation for adsorption of ellagic, gallic and malic acid molecules on Fe (110). *All quantities are in (k cal mol^{-1}).

7. According to the NBO study, Ellagic acid has a stronger inhibitory efficiency due to the low energy gaps that may promote the reactivity of these molecules toward the metal surface.
8. As a result of the Langmuir adsorption isotherm, SEM, and AFM, the adsorption process has been identified as the mechanism that prevents corrosion.

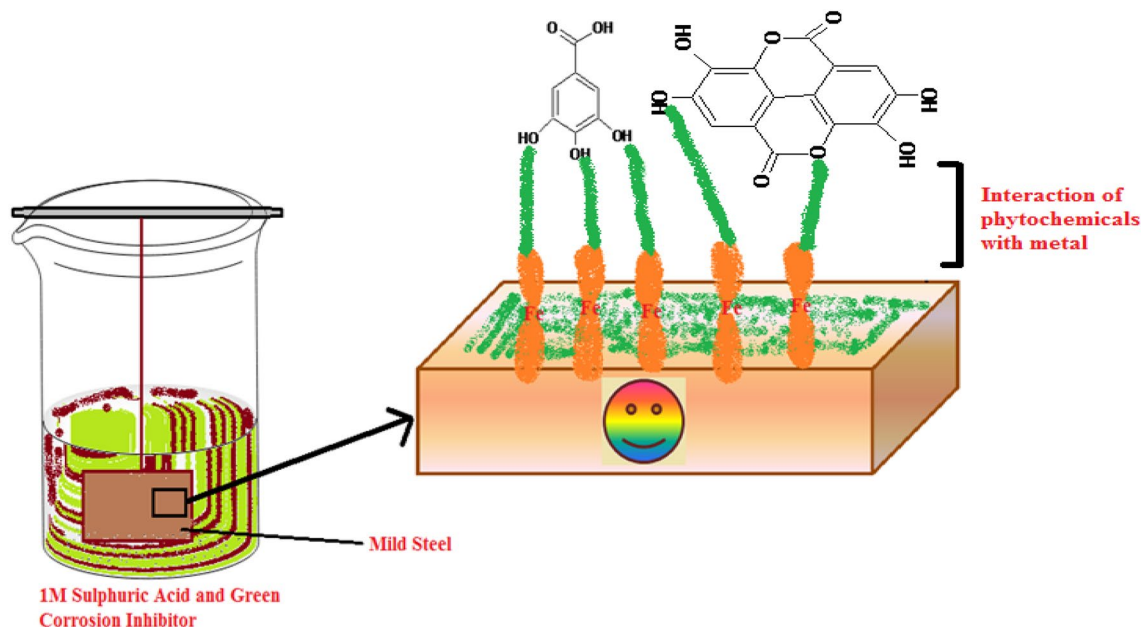


Figure 14. *Terminalia bellerica*'s phytochemical adsorption on steel to form protective layer.

Data availability

The datasets generated during and/or analyzed during the current study are available from the corresponding author on reasonable request.

Received: 20 June 2023; Accepted: 18 October 2023

Published online: 08 November 2023

References

- Bedair, M. A., Abuelela, A. M., Alshareef, M., Owda, M. & Eliwa, E. M. Ethyl ester/acyl hydrazide-based aromatic sulfonamides: Facile synthesis, structural characterization, electrochemical measurements and theoretical studies as effective corrosion inhibitors for mild steel in 1.0 M HCl. *RSC Adv.* **13**, 186–211 (2023).
- Schmitt, G. A. *et al.* Global needs for knowledge development in materials deterioration and corrosion control in cooperation with. *Fed. Highw. Adm. FHWA-RD-01*, 1–44 (2009).
- Groenewold, G. S. *et al.* Characterization of arsenic contamination on rust from ton containers. *Ind. Eng. Chem. Res.* **52**, 1396–1404 (2013).
- van der Lugt, W. *et al.* Growth of *Legionella anisa* in a model drinking water system to evaluate different shower outlets and the impact of cast iron rust. *Int. J. Hyg. Environ. Health* **220**, 1295–1308 (2017).
- Alarfaji, S. S., Ali, I. H., Bani-Fwaz, M. Z. & Bedair, M. A. Synthesis and assessment of two malonyl dihydrazide derivatives as corrosion inhibitors for carbon steel in acidic media: Experimental and theoretical studies. *Molecules* **26**, 3183 (2021).
- El-Hashemy, M. A. & Sallam, A. The inhibitive action of *Calendula officinalis* flower heads extract for mild steel corrosion in 1 M HCl solution. *J. Mater. Res. Technol.* **9**, 13509–13523 (2020).
- Chung, I.-M. *et al.* Inhibition of mild steel corrosion using *Magnolia kobus* extract in sulphuric acid medium. *Mater. Today Commun.* **25**, 101687 (2020).
- Ahanotu, C. C. *et al.* Pterocarpus santalinoides leaves extract as a sustainable and potent inhibitor for low carbon steel in a simulated pickling medium. *Sustain. Chem. Pharm.* **15**, 100196 (2020).
- Saxena, A., Thakur, K. K. & Bhardwaj, N. Electrochemical studies and surface examination of low carbon steel by applying the extract of *Musa acuminata*. *Surf. Interfaces* **18**, 100436 (2020).
- Zakaria, K., Abbas, M. A. & Bedair, M. A. Herbal expired drug bearing glycosides and polysaccharides moieties as green and cost-effective oilfield corrosion inhibitor: Electrochemical and computational studies. *J. Mol. Liq.* **352**, 118689 (2022).
- Haldhar, R. *et al.* Papaver somniferum as an efficient corrosion inhibitor for iron alloy in acidic condition: DFT, MC simulation, LCMS and electrochemical studies. *J. Mol. Struct.* **1242**, 130822 (2021).
- Parthipan, P. *et al.* *Allium sativum* (garlic extract) as a green corrosion inhibitor with biocidal properties for the control of MIC in carbon steel and stainless steel in oilfield environments. *Int. Biodeterior. Biodegrad.* **132**, 66–73 (2018).
- Saxena, A., Prasad, D., Haldhar, R., Singh, G. & Kumar, A. Use of *Sida cordifolia* extract as green corrosion inhibitor for mild steel in 0.5 M H₂SO₄. *J. Environ. Chem. Eng.* **6**, 694–700 (2018).
- Saxena, A., Prasad, D., Haldhar, R., Singh, G. & Kumar, A. Use of *Saraca ashoka* extract as green corrosion inhibitor for mild steel in 0.5 M H₂SO₄. *J. Mol. Liq.* **258**, 89–97 (2018).
- Saxena, A., Prasad, D. & Haldhar, R. Investigation of corrosion inhibition effect and adsorption activities of *Cuscuta reflexa* extract for mild steel in 0.5 M H₂SO₄. *Bioelectrochemistry* **124**, 156–164 (2018).
- Haldhar, R., Prasad, D. & Saxena, A. *Armoracia rusticana* as sustainable and eco-friendly corrosion inhibitor for mild steel in 0.5 M sulphuric acid: Experimental and theoretical investigations. *J. Environ. Chem. Eng.* **6**, 5230–5238 (2018).
- Haldhar, R., Prasad, D. & Saxena, A. *Myristica fragrans* extract as an eco-friendly corrosion inhibitor for mild steel in 0.5 M H₂SO₄ solution. *J. Environ. Chem. Eng.* **6**, 2290–2301 (2018).
- Alibakhshi, E. *et al.* *Glycyrrhiza glabra* leaves extract as a green corrosion inhibitor for mild steel in 1 M hydrochloric acid solution: Experimental, molecular dynamics, Monte Carlo and quantum mechanics study. *J. Mol. Liq.* **255**, 185–198 (2018).

19. Satapathy, A. K., Gunasekaran, G., Sahoo, S. C., Amit, K. & Rodrigues, P. V. Corrosion inhibition by *Justicia gendarussa* plant extract in hydrochloric acid solution. *Corros. Sci.* **51**, 2848–2856 (2009).
20. Chauhan, L. R. & Gunasekaran, G. Corrosion inhibition of mild steel by plant extract in dilute HCl medium. *Corros. Sci.* **49**, 1143–1161 (2007).
21. El-Etre, A. Y. Khillah extract as inhibitor for acid corrosion of SX 316 steel. *Appl. Surf. Sci.* **252**, 8521–8525 (2006).
22. Oguzie, E. E. Studies on the inhibitive effect of *Occimum viridis* extract on the acid corrosion of mild steel. *Mater. Chem. Phys.* **99**, 441–446 (2006).
23. El-Etre, A. Y., Abdallah, M. & El-Tantawy, Z. E. Corrosion inhibition of some metals using lawsonia extract. *Corros. Sci.* **47**, 385–395 (2005).
24. Bhawsar, J., Jain, P. K. & Jain, P. Experimental and computational studies of *Nicotiana tabacum* leaves extract as green corrosion inhibitor for mild steel in acidic medium. *Alex. Eng. J.* **54**, 769–775 (2015).
25. Ngouné, B., Pengou, M., Nouteza, A. M., Nanseu-Njiki, C. P. & Ngameni, E. Performances of alkaloid extract from *Rauvolfia macrophylla* stapf toward corrosion inhibition of C38 steel in acidic media. *ACS Omega* **4**, 9081–9091 (2019).
26. Prabaharan, M., Kim, S.-H., Hemapriya, V. & Chung, I.-M. Evaluation of polyphenol composition and anti-corrosion properties of *Cryptostegia grandiflora* plant extract on mild steel in acidic medium. *J. Ind. Eng. Chem.* **37**, 47–56 (2016).
27. Hassan, K. H., Khadam, A. A. & Kurshed, N. H. *Citrus aurantium* leaves extracts as a sustainable corrosion inhibitor of mild steel in sulfuric acid. *S. Afr. J. Chem. Eng.* **22**, 1–5 (2016).
28. Uwah, I. E., Okafor, P. C. & Ebiekpe, V. E. Inhibitive action of ethanol extracts from *Nauclea latifolia* on the corrosion of mild steel in H₂SO₄ solutions and their adsorption characteristics. *Arab. J. Chem.* **6**, 285–293 (2013).
29. Umoren, S. A. *et al.* Inhibition of mild steel corrosion in acidic medium using coconut coir dust extracted from water and methanol as solvents. *J. Ind. Eng. Chem.* **20**, 3612–3622 (2014).
30. Bagga, M. K. *et al.* Investigation of phytochemical components and corrosion inhibition property of *Ficus racemosa* stem extract on mild steel in H₂SO₄ medium. *J. Environ. Chem. Eng.* **4**, 4699–4707 (2016).
31. Haldhar, R. *et al.* Anticorrosive properties of a green and sustainable inhibitor from leaves extract of *Cannabis sativa* plant: Experimental and theoretical approach. *Colloids Surf. A Physicochem. Eng. Asp.* **614**, 126211 (2021).
32. Patel, N. & Šnita, D. Ethanol extracts of *Hemidesmus indicus* leaves as eco-friendly inhibitor of mild steel corrosion in H₂SO₄ medium. *Chem. Pap.* **68**, 1747 (2014).
33. Ramananda Singh, M. A green approach: A corrosion inhibition of mild steel by *Adhatoda vasica* plant extract in 0.5 M H₂SO₄. *J. Mater. Environ. Sci.* **4**, 117–126 (2013).
34. Dehghani, A., Bahlakeh, G., Ramezanzadeh, B. & Ramezanzadeh, M. A combined experimental and theoretical study of green corrosion inhibition of mild steel in HCl solution by aqueous *Citrullus lanatus* fruit (CLF) extract. *J. Mol. Liq.* **279**, 603–624 (2019).
35. Dehghani, A., Bahlakeh, G. & Ramezanzadeh, B. Green Eucalyptus leaf extract: A potent source of bio-active corrosion inhibitors for mild steel. *Bioelectrochemistry* **130**, 107339 (2019).
36. Dehghani, A., Bahlakeh, G. & Ramezanzadeh, B. A detailed electrochemical/theoretical exploration of the aqueous Chinese gooseberry fruit shell extract as a green and cheap corrosion inhibitor for mild steel in acidic solution. *J. Mol. Liq.* **282**, 366–384 (2019).
37. Dehghani, A., Bahlakeh, G., Ramezanzadeh, B. & Ramezanzadeh, M. Potential of Borage flower aqueous extract as an environmentally sustainable corrosion inhibitor for acid corrosion of mild steel: Electrochemical and theoretical studies. *J. Mol. Liq.* **277**, 895–911 (2019).
38. Benarioua, M., Mihi, A., Bouzeghaia, N. & Naoun, M. Mild steel corrosion inhibition by Parsley (*Petroselinum sativum*) extract in acidic media. *Egypt. J. Pet.* **28**, 155–159 (2019).
39. Muthukrishnan, P., Jayaprabha, B. & Prakash, P. Adsorption and corrosion inhibiting behavior of *Lannea coromandelica* leaf extract on mild steel corrosion. *Arab. J. Chem.* **10**, S2343–S2354 (2017).
40. Mehdi-pour, M., Ramezanzadeh, B. & Arman, S. Y. Electrochemical noise investigation of Aloe plant extract as green inhibitor on the corrosion of stainless steel in 1 M H₂SO₄. *J. Ind. Eng. Chem.* **21**, 318–327 (2015).
41. Gupta, A., Kumar, R., Bhattacharyya, P., Bishayee, A. & Pandey, A. K. *Terminalia bellirica* (Gaertn.) roxb. (Bahera) in health and disease: A systematic and comprehensive review. *Phytomedicine* **77**, 153278 (2020).
42. Dhanani, T., Shah, S. & Kumar, S. A validated high-performance liquid chromatography method for determination of tannin-related marker constituents gallic acid, corilagin, chebulagic acid, ellagic acid and chebulinic acid in four terminalia species from India. *J. Chromatogr. Sci.* **53**, 625–632 (2015).
43. Bedair, M. *et al.* Extracts of mint and tea as green corrosion inhibitors for mild steel in hydrochloric acid solution. *Al-Azhar Bull. Sci.* **26**, 1–14 (2015).
44. Hassan, A. *et al.* Synthesis of some triazole Schiff base derivatives and their metal complexes under microwave irradiation and evaluation of their corrosion inhibition and biological activity. *Egypt. J. Chem.* <https://doi.org/10.21608/ejchem.2019.10834.1699> (2019).
45. Junaedi, S., Al-Amiery, A., Kadhim, A., Kadhum, A. & Mohamad, A. Inhibition effects of a synthesized novel 4-aminoantipyrine derivative on the corrosion of mild steel in hydrochloric acid solution together with quantum chemical studies. *Int. J. Mol. Sci.* **14**, 11915–11928 (2013).
46. Scully, J. R. Polarization resistance method for determination of instantaneous corrosion rates. *Corrosion* **56**, 199–218 (2000).
47. Majeed, M. N., Yousif, Q. A. & Bedair, M. A. Study of the corrosion of nickel–chromium alloy in an acidic solution protected by nickel nanoparticles. *ACS Omega* **7**, 29850–29857 (2022).
48. Yousif, Q. A. *et al.* Insight into the corrosion mitigation performance of three novel benzimidazole derivatives of amino acids for carbon steel (X56) in 1 M HCl solution. *RSC Adv.* **13**, 13094–13119 (2023).
49. Elaryian, H. M., Bedair, M. A., Bedair, A. H., Aboushahba, R. M. & Fouda, A. E.-A. S. Synthesis, characterization of novel coumarin dyes as corrosion inhibitors for mild steel in acidic environment: Experimental, theoretical, and biological studies. *J. Mol. Liq.* **346**, 118310 (2022).
50. Frisch, M. J. *Gaussian 09* (Gaussian Inc, 2009).
51. Becke, A. D. A new mixing of Hartree–Fock and local density-functional theories. *J. Chem. Phys.* **98**, 1372 (1993).
52. Lee, C., Yang, W. & Parr, R. G. Development of the Colle–Salvetti correlation-energy formula into a functional of the electron density. *Phys. Rev. B* **37**, 785–789 (1988).
53. Vosko, S. H., Wilk, L. & Nusair, M. Accurate spin-dependent electron liquid correlation energies for local spin density calculations: A critical analysis. *Can. J. Phys.* **58**, 1200–1211 (1980).
54. Dennington, R., Keith, T. A. & Millam, J. M. *GaussView 6* (Semicem Inc, 2016).
55. Zhang, G. & Musgrave, C. B. Comparison of DFT methods for molecular orbital eigenvalue calculations. *J. Phys. Chem. A* **111**, 1554–1561 (2007).
56. Pearson, R. G. *Chemical Hardness* (Wiley-VCH Verlag GmbH, 1997).
57. Bedair, M. A., Abuelela, A. M., Zoghaib, W. M. & Mohamed, T. A. Molecular structure, tautomer's, reactivity and inhibition studies on 6-methyl-2-thiouracil for mild steel corrosion in aqueous HCl (1.00 M): Experimental and theoretical studies. *J. Mol. Struct.* **1244**, 130927 (2021).
58. Glendening, E. D., Reed, A. E., Carpenter, J. E. & Weinhold, F. *NBO Version 3.1*. (2016).
59. *Adsorption Locator Module Built in Materials Studio*. (BIOVIA, 2017).

60. Abbas, M. A. *et al.* Performance assessment by experimental and theoretical approaches of newly synthesized benzyl amide derivatives as corrosion inhibitors for carbon steel in 1.0 M hydrochloric acid environment. *Inorg. Chem. Commun.* **143**, 109758 (2022).
61. Awad, M. K., Metwally, M. S., Soliman, S. A., El-Zomrawy, A. A. & Bedair, M. A. Experimental and quantum chemical studies of the effect of poly ethylene glycol as corrosion inhibitors of aluminum surface. *J. Ind. Eng. Chem.* **20**, 796–808 (2014).
62. Elaryian, H. M., Bedair, M. A., Bedair, A. H., Aboushabha, R. M. & Fouda, A.E.-A.S. Corrosion mitigation for steel in acid environment using novel p-phenylenediamine and benzidine coumarin derivatives: Synthesis, electrochemical, computational and SRB biological resistivity. *RSC Adv.* **12**, 29350–29374 (2022).
63. Bedair, M. A., Soliman, S. A. & Metwally, M. S. Synthesis and characterization of some nonionic surfactants as corrosion inhibitors for steel in 1.0 M HCl (experimental and computational study). *J. Ind. Eng. Chem.* **41**, 10–22 (2016).
64. Bedair, M. A. *et al.* Insights into the adsorption and corrosion inhibition properties of newly synthesized diazinyll derivatives for mild steel in hydrochloric acid: Synthesis, electrochemical, SRB biological resistivity and quantum chemical calculations. *RSC Adv.* **13**, 478–498 (2023).
65. Bedair, M. A. *et al.* Novel coumarin-buta-1,3-diene conjugated donor–acceptor systems as corrosion inhibitors for mild steel in 1.0 M HCl: Synthesis, electrochemical, computational and SRB biological resistivity. *Inorg. Chem. Commun.* **148**, 110304 (2023).
66. Ashmawy, A. M., Said, R., Naguib, I. A., Yao, B. & Bedair, M. A. Anticorrosion study for brass alloys in heat exchangers during acid cleaning using novel Gemini surfactants based on benzalkonium tetrafluoroborate. *ACS Omega* **7**, 17849–17860 (2022).
67. Abbas, M. A. & Bedair, M. A. Adsorption and computational studies for evaluating the behavior of silicon based compounds as novel corrosion inhibitors of carbon steel surfaces in acidic media. *Z. Phys. Chem.* **233**, 225–254 (2019).
68. Abbas, M. A., Bedair, M. A., El-Azabawy, O. E. & Gad, E. S. Anticorrosion effect of ethoxylate sulfanilamide compounds on carbon steel in 1 M hydrochloric acid: Electrochemical and theoretical studies. *ACS Omega* **6**, 15089–15102 (2021).
69. Bedair, M. A., Alosaimi, E. H. & Melhi, S. A study of the inhibitive effect for corrosion of steel in 1.0 M HCl using a new nonionic surfactant based on coumarin moiety: Chemical, electrochemical and quantum mechanics calculations. *J. Adhes. Sci. Technol.* <https://doi.org/10.1080/01694243.2021.2018864> (2021).
70. Abdelsalam, M. M. *et al.* Green synthesis, electrochemical, and DFT studies on the corrosion inhibition of steel by some novel triazole Schiff base derivatives in hydrochloric acid solution. *Arab. J. Chem.* **15**, 103491 (2022).
71. El-Sabbah, M. M. B. *et al.* Synergistic effect between natural honey and 0.1 M KI as green corrosion inhibitor for steel in acid medium. *Z. Phys. Chem.* **233**, 627–649 (2019).
72. Shabani-Nooshabadi, M. & Ghandchi, M. S. Santolina chamaecyparissus extract as a natural source inhibitor for 304 stainless steel corrosion in 3.5% NaCl. *J. Ind. Eng. Chem.* **31**, 231–237 (2015).
73. Ferreira, E., Giacomelli, C., Giacomelli, F. & Spinelli, A. Evaluation of the inhibitor effect of l-ascorbic acid on the corrosion of mild steel. *Mater. Chem. Phys.* **83**, 129–134 (2004).
74. Yousef, Q. A., Majeed, M. N. & Bedair, M. A. Surface protection against corrosion of Ni turbine blades by electrophoretic deposition of MnO₂, TiO₂ and TiO₂-C nanocoating. *RSC Adv.* **12**, 33725–33736 (2022).
75. Ragab, M. & Bedair, M. A. The effect of permanent magnet stirring on the corrosion resistance of Sn-2.0Ag-0.5Cu-2Zn solder alloys in NaCl solution. *Mater. Chem. Phys.* **302**, 127774 (2023).
76. Ahmed, A. S., Mohamed, M. B. I., Bedair, M. A., El-Zomrawy, A. A. & Bakr, M. F. A new Schiff base-fabricated pencil lead electrode for the efficient detection of copper, lead, and cadmium ions in aqueous media. *RSC Adv.* **13**, 15651–15666 (2023).
77. Melhi, S. *et al.* Effective corrosion inhibition of mild steel in hydrochloric acid by newly synthesized Schiff base nano Co(II) and Cr(III) complexes: Spectral, thermal, electrochemical and DFT (FMO, NBO) studies. *RSC Adv.* **12**, 32488–32507 (2022).
78. Bedair, M. A. *et al.* Benzidine-based Schiff base compounds for employing as corrosion inhibitors for carbon steel in 1.0 M HCl aqueous media by chemical, electrochemical and computational methods. *J. Mol. Liq.* **317**, 114015 (2020).
79. Pandey, A., Tripathi, S. & Pandey, C. A. Concept of standardization, extraction and pre phytochemical screening strategies for herbal drug. *J. Pharmacogn. Phytochem. JPP* **115**, 115–119 (2014).
80. Ismail, A. M. *et al.* Preliminary phytochemical screening, plant growth inhibition and antimicrobial activity studies of *Faidherbia albida* legume extracts. *J. Saudi Soc. Agric. Sci.* **15**, 112–117 (2016).
81. Alqethami, A. & Aldhebiani, A. Y. Medicinal plants used in Jeddah, Saudi Arabia: Phytochemical screening. *Saudi J. Biol. Sci.* **28**, 805–812 (2021).
82. Kumar, J., Kaur, A. & Narang, P. Phytochemical screening and metal binding studies on floral extract of *Solanum nigrum*. *Mater. Today Proc.* **26**, 3332–3336 (2020).
83. Bedair, M. A., El-Sabbah, M. M. B., Fouda, A. S. & Elaryian, H. M. Synthesis, electrochemical and quantum chemical studies of some prepared surfactants based on azodye and Schiff base as corrosion inhibitors for steel in acid medium. *Corros. Sci.* **128**, 54–72 (2017).
84. Abbas, M. A. *et al.* Synthesis, characterization, thermodynamic analysis and quantum chemical approach of branched N, N'-bis(p-hydroxybenzoyl)-based propanediamine and triethylenetetramine for carbon steel corrosion inhibition in hydrochloric acid medium. *Arab. J. Sci. Eng.* <https://doi.org/10.1007/s13369-022-07520-y> (2022).
85. Gebril, M. A., Bedair, M. A., Soliman, S. A., Bakr, M. F. & Mohamed, M. B. I. Experimental and computational studies of the influence of non-ionic surfactants with coumarin moiety as corrosion inhibitors for carbon steel in 1.0 M HCl. *J. Mol. Liq.* **349**, 118445 (2022).
86. Elsenety, M. M., Elsayed, B. A., Ibrahim, I. A. & Bedair, M. A. Photophysical, DFT and molecular docking studies of Sm(III) and Eu(III) complexes of newly synthesized coumarin ligand. *Inorg. Chem. Commun.* **121**, 108213 (2020).
87. Mostafa, M. A., Ashmawy, A. M., Reheim, M. A. M. A., Bedair, M. A. & Abuelela, A. M. Molecular structure aspects and molecular reactivity of some triazole derivatives for corrosion inhibition of aluminum in 1 M HCl solution. *J. Mol. Struct.* **1236**, 130292 (2021).
88. Abuelela, A. M., Bedair, M. A., Zoghaib, W. M., Wilson, L. D. & Mohamed, T. A. Molecular structure and mild steel/HCl corrosion inhibition of 4,5-Dicyanoimidazole: Vibrational, electrochemical and quantum mechanical calculations. *J. Mol. Struct.* **1230**, 129647 (2021).
89. Badr, E. A., Bedair, M. A. & Shaban, S. M. Adsorption and performance assessment of some imine derivatives as mild steel corrosion inhibitors in 1.0 M HCl solution by chemical, electrochemical and computational methods. *Mater. Chem. Phys.* **219**, 444–460 (2018).
90. Soliman, S. A., Metwally, M. S., Selim, S. R., Bedair, M. A. & Abbas, M. A. Corrosion inhibition and adsorption behavior of new Schiff base surfactant on steel in acidic environment: Experimental and theoretical studies. *J. Ind. Eng. Chem.* **20**, 4311–4320 (2014).
91. Bedair, M. A., Fouda, A. S., Ismail, M. A. & Mostafa, A. Inhibitive effect of bithiophene carbonitrile derivatives on carbon steel corrosion in 1 M HCl solution: experimental and theoretical approaches. *Ionics (Kiel)*. **25**, 2913–2933 (2019).
92. Bedair, M. A., Soliman, S. A., Hegazy, M. A., Obot, I. B. & Ahmed, A. S. Empirical and theoretical investigations on the corrosion inhibition characteristics of mild steel by three new Schiff base derivatives. *J. Adhes. Sci. Technol.* **33**, 1139–1168 (2019).
93. Bedair, M. A. The effect of structure parameters on the corrosion inhibition effect of some heterocyclic nitrogen organic compounds. *J. Mol. Liq.* **219**, 128–141 (2016).
94. Vashishth, P., Bairagi, H., Narang, R., Shukla, S. K. & Mangla, B. Thermodynamic and electrochemical investigation of inhibition efficiency of green corrosion inhibitor and its comparison with synthetic dyes on MS in acidic medium. *J. Mol. Liq.* **365**, 120042 (2022).

Acknowledgements

This work was supported by the Deanship of Scientific Research, Vice Presidency for Graduate Studies and Scientific Research, King Faisal University, Saudi Arabia [GRANT4706]. Mahmoud A. Bedair also thanks the Deanship of Scientific Research at University of Bisha for supporting this work through the Fast-Track Research Support Program.

Author contributions

A.M.A. and M.A.B.: Investigation, Experimental, Computational analysis, Data Curation for inhibitor efficiency, Writing-Original Draft and Resources, J.K. and A.S.: Conceptualization, Experimental, Validation, Formal Analysis, Writing-Original Draft, D.K.V. and E.B.: Investigation, Experimental, Data Curation for inhibitor efficiency and Resources.

Funding

This work was supported by the Deanship of Scientific Research, Vice Presidency for Graduate Studies and Scientific Research, King Faisal University, Saudi Arabia [GRANT4706].

Competing interests

The authors declare no competing interests.

Additional information

Supplementary Information The online version contains supplementary material available at <https://doi.org/10.1038/s41598-023-45283-0>.

Correspondence and requests for materials should be addressed to A.M.A., A.S. or M.A.B.

Reprints and permissions information is available at www.nature.com/reprints.

Publisher's note Springer Nature remains neutral with regard to jurisdictional claims in published maps and institutional affiliations.



Open Access This article is licensed under a Creative Commons Attribution 4.0 International License, which permits use, sharing, adaptation, distribution and reproduction in any medium or format, as long as you give appropriate credit to the original author(s) and the source, provide a link to the Creative Commons licence, and indicate if changes were made. The images or other third party material in this article are included in the article's Creative Commons licence, unless indicated otherwise in a credit line to the material. If material is not included in the article's Creative Commons licence and your intended use is not permitted by statutory regulation or exceeds the permitted use, you will need to obtain permission directly from the copyright holder. To view a copy of this licence, visit <http://creativecommons.org/licenses/by/4.0/>.

© The Author(s) 2023